SANDIA REPORT

SAND95-1887 • UC-814
Unlimited Release
Printed September 1997

Yucca Mountain Site Characterization Project

The Effects of Confining Pressure on the Strength and Elastic Properties of the Paintbrush Tuff Recovered from Boreholes USW NRG-6 and USW NRG-7/7A: Data Report

R. J. Martin, J. S. Noel, P. J. Boyd, R. H. Price

Prepared by
Sandia National Laboratories
Albuquerque, New Mexico 87185 and Livermore, California 94550

Sandia is a multiprogram laboratory operated by Sandia Corporation, a Lockheed Martin Company, for the United States Department of Energy under Contract DE-AC04-94AL85000.

Sandia National Laboratories

"Prepared by Yucca Mountain Site Characterization Project (YMSCP) participants as part of the Civilian Radioactive Waste Management Program (CRWM). The YMSCP is managed by the Yucca Mountain Project Office of the U.S. Department of Energy, DOE Field Office, Nevada (DOE/NV). YMSCP work is sponsored by the Office of Geologic Repositories (OGR) of the DOE Office of Civilian Radioactive Waste Management (OCRWM)."

Issued by Sandia National Laboratories, operated for the United States Department of Energy by Sandia Corporation.

Available to DOE and DOE contractors from
Office of Scientific and Technical Information
P.O. Box 62
Oak Ridge, TN 37831

Prices available from (615) 576-8401, FTS 626-8401

Available to the public from
National Technical Information Service
U.S. Department of Commerce
5285 Port Royal Rd
Springfield, VA 22161

NTIS price codes
Printed copy: A04
Microfiche copy: A01

SAND95-1887
Unlimited Release
Printed September 1997

Distribution
Category UC-814

The Effects of Confining Pressure on the Strength and Elastic Properties of the Paintbrush Tuff Recovered from Boreholes USW NRG-6 and USW NRG-7/7A: Data Report

R. J. Martin, J. S. Noel, P. J. Boyd
New England Research, Inc.
White River Junction, Vermont 05001

R. H. Price
YMP Performance Assessment Applications Department
Sandia National Laboratories
P.O. Box 5800
Albuquerque, New Mexico 87185-1325

ABSTRACT

Experimental results are presented for bulk and mechanical properties measurements on specimens of the Paintbrush tuff recovered from the USW NRG-6 and USW NRG-7/7A boreholes at Yucca Mountain, Nevada. Measurements have been performed on five thermal/mechanical units: TCw, PTn, TSw2, and TSw3. The following bulk properties are reported for each specimen: dry bulk density, saturated bulk density, average grain density and porosity. Confined compression to failure tests were performed on selected specimens recovered from the boreholes at confining pressures of 5 and 10 MPa. In addition, compressional and shear wave velocities were measured on the specimens prior to testing. Measurements were conducted under drained conditions at room temperature on nominally water saturated specimens. The nominal strain rate for the experiments was 10^{-5} s^{-1}.

CONTENTS

List of Figures

List of Tables

This report was prepared for the Yucca Mountain Site Characterization Project. The scientific investigation discussed in this report is covered under the description of work for WBS number 1.2.3.2.7.1.3, QA Grading Report #1.2.3.2.7.1.3, Revision 00. The planning documents that guided this work activity are Site Characterization Plan Section 8.3.1.15.1.3; Study Plan SP-8.3.1.15.1.3, Revision 0; and Work Agreement WA-0090. The information and data documented in this report were collected under a fully qualified QA Program and may be used in the licensing process. The data contained in this report has been submitted on TDIFs #304095 and #304135.

1.0 INTRODUCTION

An integral part of the licensing procedure for the potential nuclear waste repository at Yucca Mountain, Nevada, involves prediction of the *in situ* rheology for the design and construction of the facility and the emplacement of canisters containing radioactive waste. The data used to model the thermal and mechanical behavior of the repository and surrounding lithologies include dry and saturated bulk densities, average grain density, porosity, compressional and shear wave velocities, elastic moduli, and compressional and tensional fracture strengths. In this study, a suite of confined compression and bulk property measurements were performed on cores recovered from the USW NRG-6 and USW NRG-7/7A boreholes drilled in support of the Exploratory Studies Facility (ESF) at Yucca Mountain. USW NRG-6 was drilled to a depth of 1,100.0 feet, terminating in the TSw2 thermal/mechanical unit. USW NRG-7/7A was drilled to a depth of 1,513.4 feet through five thermal/mechanical units of Paintbrush tuff and terminated in the tuffaceous beds of the Calico Hills formation. The thermal/mechanical stratigraphy was defined by Ortiz et al. (1985) to group rock horizons of similar properties for the purpose of simplifying modeling efforts. The relationship between the geologic stratigraphy and the thermal/mechanical stratigraphy is presented in Figures 1 and 2. The tuff samples in this study have a wide range of welding characteristics (usually reflected in sample porosity), and a smaller range of mineralogy and petrology characteristics. Generally, the samples are silicic, ash-fall tuffs that exhibit large variability in their elastic and strength properties (see Price and Bauer, 1985).

Thirty-nine cores from USW NRG-6 and USW NRG-7/7A were sent to New England Research, Inc., for bulk property measurements and baseline mechanical property measurements under confined compression conditions. A breakdown of the samples according to tests performed is given below:

Type of Test	**Number of Samples Tested**
Average Grain Density	39
Confined Compression	23

On sixteen (16) cores there was insufficient material or the material was of such poor quality that mechanical tests could not be performed. On these cores, only average grain density and porosity were determined.

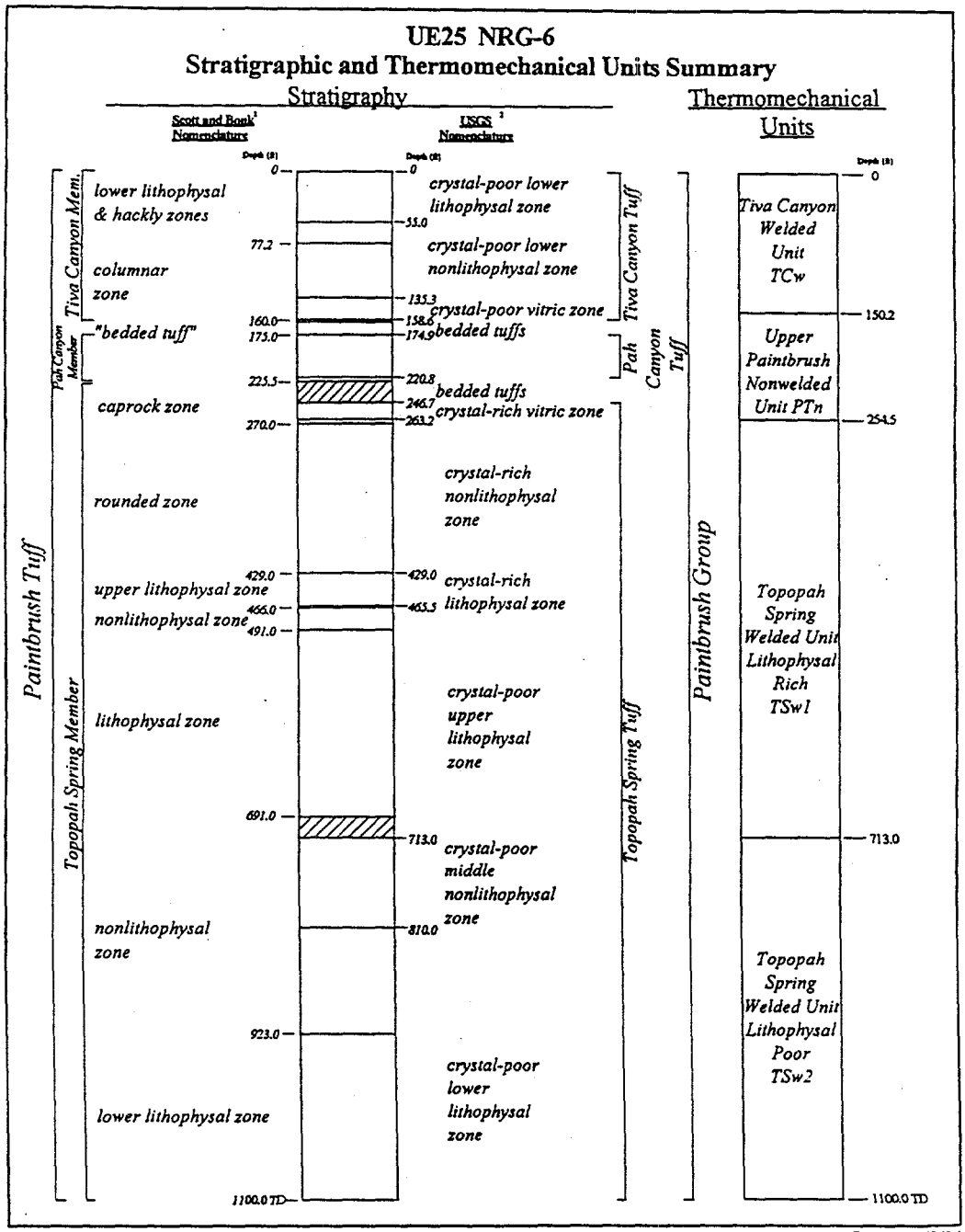

Unresolved contact showing difference between criteria. Solid line shows contact based on Scott & Bonk [1]; dashed line is contact based on USGS [2].

Date: 12/9/94

[1] U. S. Geological Survey - Preliminary Geologic Map of Yucca Mountain, Nye County, Nevada, With Geologic Sections, Robert B. Scott and Jerry Bonk, USGS Open File Report 84-494.

[2] U. S. Geological Survey - Graphical Lithologic Log of Borehole NRG-6, Thomas Moyer and Jeff Geslin, DTN:GS931008314211.045.

Figure 1: The correlation between the stratigraphic and thermal/mechanical units for borehole USW NRG-6 at Yucca Mountain, Nevada (Brechtel et al. 1995).

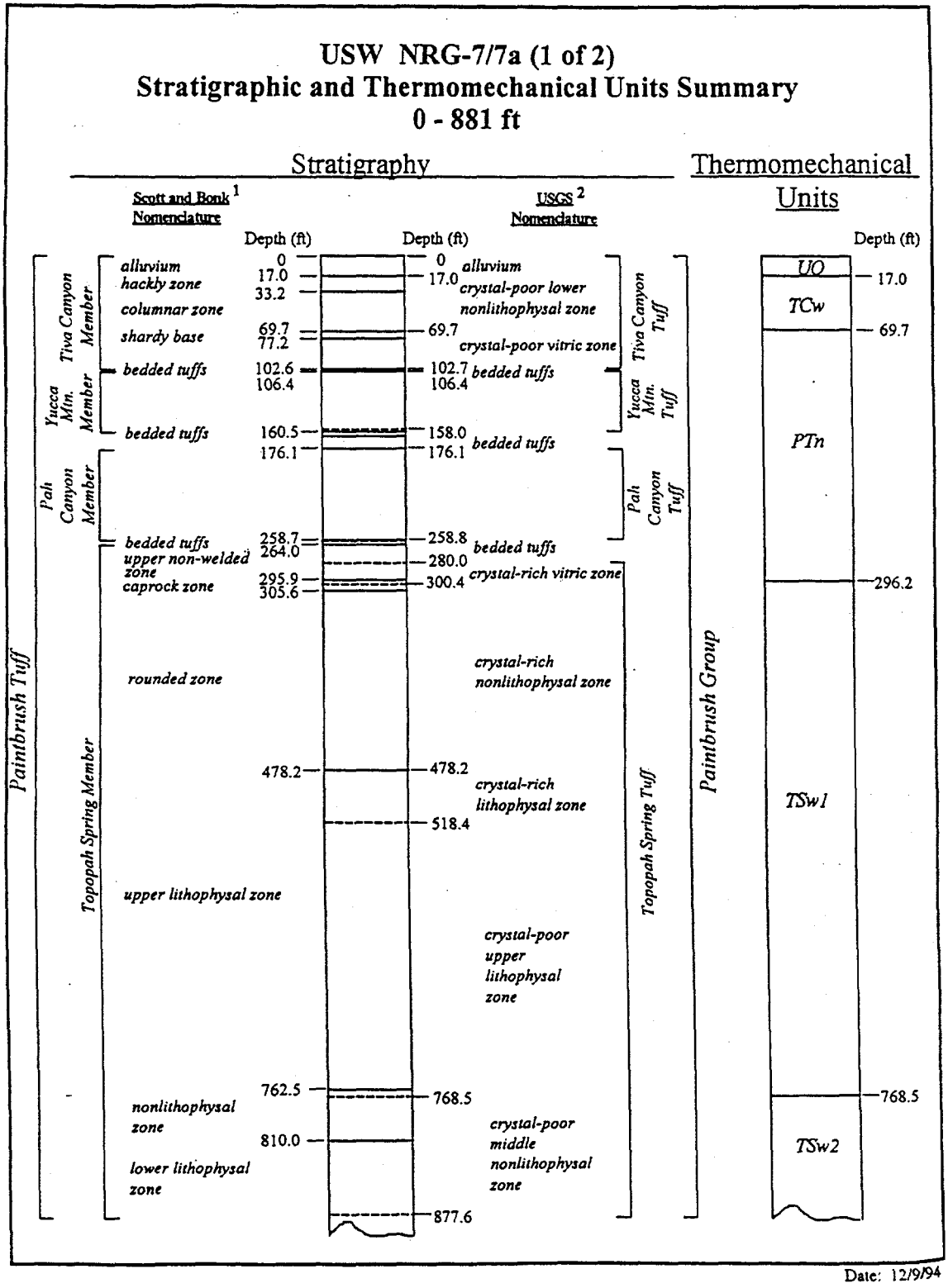

Figure 2: The correlation between the stratigraphic and thermal/mechanical units for borehole USW NRG-7/7A at Yucca Mountain, Nevada (Brechtel et al. 1995).

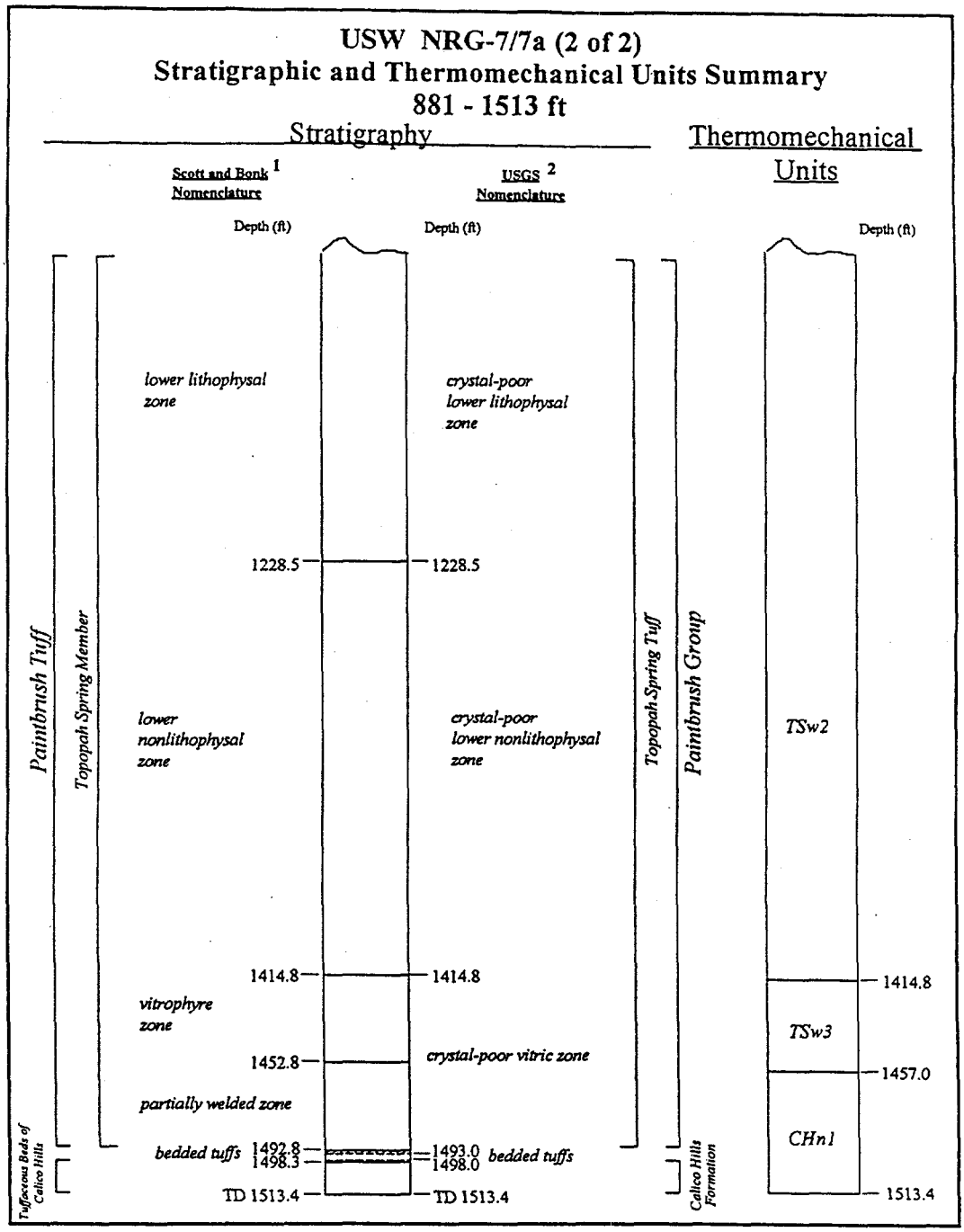

Unresolved contact showing difference between criteria. Solid line shows contact based on Scott & Bonk [1]; dashed line is contact based on USGS [2].

Date: 12/9/94

1 U. S. Geological Survey - Preliminary Geologic Map of Yucca Mountain, Nye County, Nevada, With Geologic Sections, Robert B. Scott and Jerry Bonk, USGS Open File Report 84-494.

2 U. S. Geological Survey - Graphical Lithologic Log of Borehole NRG-7/7a, Thomas Moyer and Jeff Geslin, DTN:GS940408314211.020.

Figure 2 (continued): The correlation between the stratigraphic and thermal/mechanical units for borehole USW NRG-7/7A at Yucca Mountain, Nevada (Brechtel et al. 1995).

2.0 EXPERIMENTAL PROCEDURE

Confined compression tests were performed on 23 specimens prepared from core recovered from boreholes USW NRG-6 and USW NRG-7/7A. When the core was received it was examined to determine the best utilization of the rock material to obtain the maximum mechanical data. The nominal dimensions of the cylindrical rock specimens for the confined compression tests are given below:

Test	**Length (mm)**	**Diameter (mm)**
Confined Compression	101.6	50.8

The actual length and diameter measurements of each specimen have a tolerance of ± 0.125 mm. The ends of the cylinders were parallel to within 0.025 mm.

Dry, and saturated bulk densities were measured on each of the test specimens. Average grain density was determined with the water pycnometry technique using pieces remaining from the subcoring attendant to the preparation of the test specimens.

2.1 Sample Preparation

All test specimens were ground, right circular cylinders with dimensions listed above. The dimensions of the specimens were checked and verified according to the Sandia National Laboratories (SNL) Technical Procedure (TP) 51 entitled "Preparing Cylindrical Samples, Including Inspection of Dimensional and Shape Tolerances".

The general testing sequence for each specimen is given below:

Dimensions measurement
Specimen description
Compressional and shear wave velocities for the room dry condition
Saturating specimen to a constant weight with water
Saturated bulk density measurement
Compressional and shear wave velocities for the saturated state
Confined compression testing
Description of post failure condition of the specimen
Drying specimen to a constant weight
Dry bulk density measurement
Post-test photograph taken

Average grain density measurements were performed concurrently with the other activities.

2.2 Drying, Saturation, Bulk Density, Average Grain Density, and Porosity

The dry and saturated bulk densities, average grain density and porosity were determined for each mechanical test specimen. The procedures were carried out according to SNL TP 229 entitled, "Bulk Properties Determinations of Tuffaceous Rocks: Dry Bulk Density, Saturated Bulk Density, Average Grain Density and Porosity."

2.2.1 Procedure for Water Saturation

The mechanical tests were performed on water saturated specimens. Saturation of the specimens was achieved in a two-stage process. First, the specimen was pressure saturated at 10 MPa for a minimum of 1 hour. Next, a minimum of two vacuum saturation cycles were performed, according to SNL TP-64, "Procedure for Vacuum Saturation of Geologic Core Samples." Once the mass change for successive saturation cycles had stabilized to within $\pm$ 0.05 percent, the saturated bulk density, ρ_{sb}, was computed. The specimens were stored in distilled water following saturation and prior to testing.

A brief synopsis of the procedure for saturation follows:

1) Place the specimen in a pressure vessel filled with distilled water.

2) Pressurize the vessel to 10 MPa and hold constant for at least one hour.

3) Remove the specimen from the pressure vessel, blot it with a damp lint-free paper towel.

4) Weigh the specimen within 15 seconds of blotting. Record the mass of the specimen in the laboratory notebook.

5) Submerse (completely) the specimen in a container filled with distilled water.

6) Place the water filled container with the specimen in a vacuum chamber.

7) Apply a vacuum to the vacuum chamber.

8) Vacuum saturate the specimen for at least 30 hours.

9) Turn off the vacuum pump, open the valve on the vacuum chamber and allow the pressure to equilibrate with atmospheric conditions.

10) Keep the specimen submerged in water at ambient pressure for at least 16 hours.

11) Remove the specimen from the container and blot it with a damp lint-free paper towel.

12) Weigh the specimen within 15 seconds of blotting. Record the mass of the specimen on the vacuum saturation data sheet.

13) Submerse the specimen in the water filled container and repeat steps 11 and 12. Calculate the mean saturated mass of the specimen for the two measurements.

14) Submerse the specimen in the water filled container and repeat the vacuum saturation procedure in steps 6 through 13. Calculate the mass change for each successive vacuum saturation cycle. If the mass change for successive vacuum saturation cycles is less than or equal to 0.05% the process has met the specification and the saturation procedure is terminated. If the mass change is greater than 0.05% steps 6 through 13 must be repeated until the specification is met.

15) Store the specimen in distilled water at ambient pressure and temperature until it is ready for mechanical testing.

16) Compute the saturated bulk density by dividing the saturated mass by the specimen volume (calculated from length and diameter measurements).

2.2.2 Procedure for Drying a Specimen

At the completion of the deformation tests, the tuff specimens were left in their jackets, and all particles were collected for dry bulk density analysis. The specimens were dried to a constant weight, and their dry bulk densities were determined. Drying was carried out a $110\pm5\ ^{0}C$ according to SNL TP-65, "Drying Geologic Samples to Constant Weight". Once the mass change for successive drying cycles had stabilized to within ± 0.05 percent, the dry bulk density *Pdb,* was computed.

Each specimen is dried in an oven controlled to an accuracy of ± 5 °C. The procedure for drying is outlined below.

1) Place the specimen in the oven. Increase the temperature in the oven to 110 ± 5 °C at a rate less than or equal to 2 °C min^{-1}.

2) Maintain the specimen at 110 ± 5 °C for 120 to 128 hours. Reduce the temperature in the oven at a rate of less than or equal to 2 °C min^{-1} until the oven temperature is between ambient and 40 °C.

3) Remove the specimen from the drying oven and weigh it three times. The specimen should be weighed within 15 seconds of removal from the oven. Calculate the mean dry mass of the specimen for the three measurements.

4. Repeat steps 1 through 3.

5) Calculate the mass change of the specimen for the successive drying cycles. If the change in mass for successive drying cycles is less than or equal to 0.05% the process has met the specification and oven drying of the specimen is terminated. If the mass change is greater than 0.05% steps 1 through 3 must be repeated until the specification is met.

6) Compute the dry bulk density by dividing the dry mass by the original specimen volume.

2.2.3 Average Grain Density Measurement Using Water Pycnometry

The average grain density of each core received from the USW NRG-6 and USW NRG-7/7A boreholes was measured using the water pycnometry method (Boyd et al., 1994). The technique employs a two-stage measurement. First, the mass of a dry, powdered specimen is measured. Next, the volume of the powder is determined. These two measurements are combined to compute the average grain density.

Pieces of core with a mass of approximately 20 to 50 grams are ground to a powder with a particle size of 1.5 mm or less. The powder is dried according to SNL TP-65.

The powdered specimen of tuff is added to a dry, calibrated, water pycnometer with a nominal volume of 100 ml. The step-by-step procedure presented below produces measurements of the dry mass of the powdered specimen and the corresponding volume of the specimen. The technique has been verified using quartz powders with a well characterized density.

1. Pulverize approximately 20 to 50 g of the specimen to a particle size of 1.5 mm or less. The powder is dried in an aluminum drying pan according to SNL TP-65, except cooling is not allowed at any time in order to minimize rehydration.

2. Add the dried sample to a calibrated, clean, dry and numbered pycnometer by pouring it through a clean, dry transfer funnel.

3. Weigh the pycnometer with the dry sample immediately (do not allow it to cool).

4. Add 50 to 60 ml of distilled water to the pycnometer and swirl it to moisten all of the sample powder.

5. Place the pycnometer, with the sample, in an active vacuum for a minimum of 16 hours. For the first one or two hours, watch the pycnometer to ensure that the boiling action does not displace any of the sample from the pycnometer. The vacuum should be regulated depending upon the observed phenomena.

6. Remove the pycnometer from the vacuum chamber and pour additional deaired water into the pycnometer until the water level is just below the scribe line. Note that pouring water down the neck reduces the likelihood of entrapping air into the water as it is added to the pycnometer.

7. Use a pipette to add water until the bottom of the meniscus is at the height of the scribe line. It may be necessary to raise the water level higher than the scribe line, to wet the sides of the pycnometer for a suitable meniscus. In this case, water is removed to obtain the correct reading.

8. Use a cotton swab to dry the inside of the neck of the pycnometer.

9. Use a lint free wipe to clean and dry the exterior of the pycnometer.

10. Weigh the pycnometer and its contents.

11. Measure the water temperature in the pycnometer to the nearest 0.2 ^{o}C.

12. Calculate the average grain density (ρ_g) of the specimen using the water pycnometer grain density measurement sheet.

13. Pour the sample and water into a clean container to allow the water to evaporate.

14. Store the sample powder in a container to maintain it in its original condition.

2.2.4 Dry Bulk Density, Saturated Bulk Density, and Porosity

The dry bulk density, ρ_{db}, is obtained by computing the volume of a test specimen from its external dimensions and dividing it into the mass measured in a dry condition. The density corresponding to the measurement in the saturated condition is the saturated bulk density, ρ_{sb}. Preferably, porosity, ϕ, is computed using the following relation (Boyd et al., 1994):

$$\phi = \frac{\rho_g - \rho_{db}}{\rho_g} \times 100\%$$

Alternatively, the porosity can be calculated from the dry bulk density and saturated bulk density according to (Boyd et al., 1994):

$$\phi = \frac{\rho_{sb} - \rho_{db}}{\rho_w} \times 100\%$$

where ρ_w is the density of water.

2.3 Compressional and Shear Wave Velocity Measurements

Compressional and shear wave velocities were measured on right circular cylinders with a nominal length to diameter ratio of 2:1. The velocities were measured for both room dry and water saturated conditions at ambient temperature in a benchtop apparatus.

The compressional and shear wave velocity measurements are used for two main purposes. First, a measure of the specimen anisotropy can be directly obtained by comparing the compressional and shear wave velocities measured both parallel and normal to the core axis. Second, compressional and shear wave velocity data, combined with the density of the specimen, are used to compute dynamic Young's modulus and Poisson's ratio.

A self-contained ultrasonic measuring system is used to perform the velocity measurements. A tuff specimen is placed between a matched set of ultrasonic transducers. One transducer serves as the source; the second as the receiver (Figure 3). The travel time (corrected for delays through the non-specimen components of the system) through the rock is divided by the sample length to compute the velocity.

Each ultrasonic transducer contains one compressional and one or two polarized shear wave elements. For the measurements parallel to the core axis one compressional and two

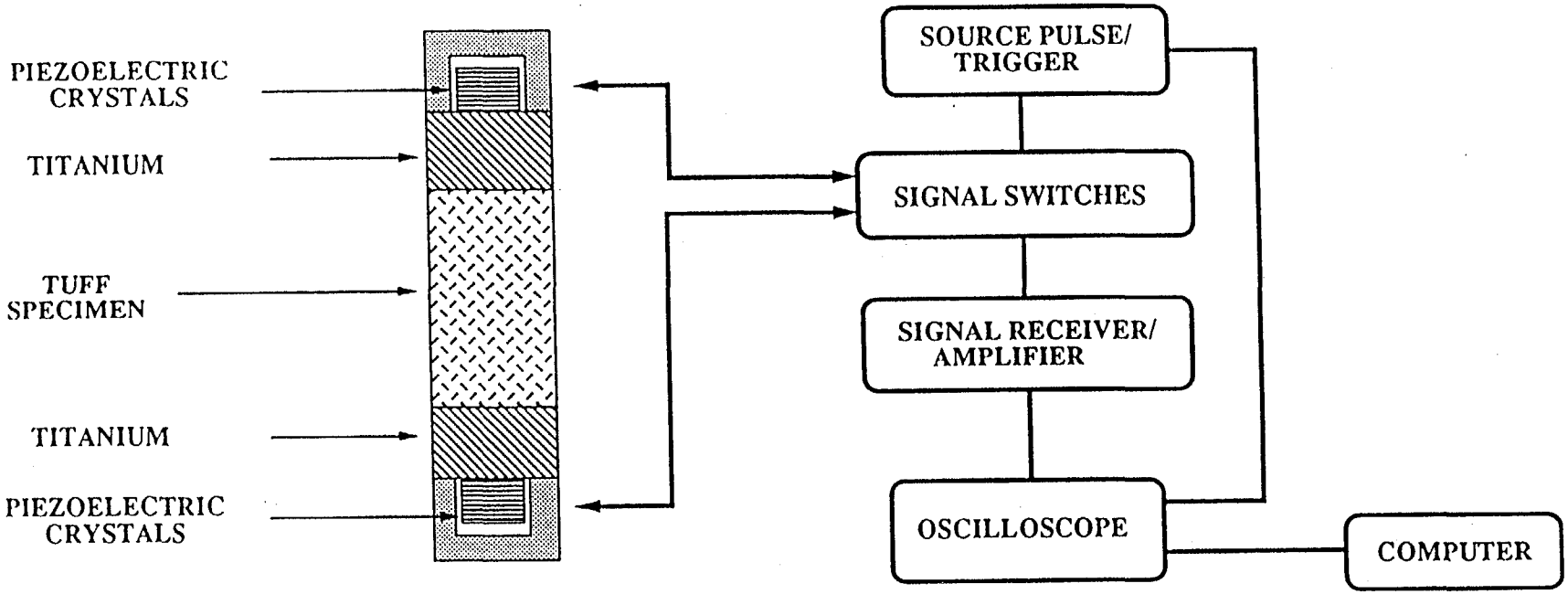

Figure 3: Schematic diagram of the geometry used to measure compressional and shear wave velocities in tuff. The diagram shows the setup for the measurement of velocities parallel to the core axis.

orthogonally polarized shear waves are propagated. For measurements normal to the core axis, one compressional and one polarized shear wave velocity are measured. The polarization direction of the shear wave propagating normal to the core axis is parallel to the axis of the core.

The transducers are constructed using piezoelectric crystals with a resonant frequency of 1 MHz. The multicomponent piezoelectric crystals are bonded to a titanium substrate. Titanium has been selected because it has a good acoustical impedance match both to the rock and to the piezoelectrical crystals. The source crystal is excited with a fast rise time pulse generator. The crystal produces a broad band ultrasonic pulse propagated through the adjacent titanium substrate, the rock, the titanium at the opposite end of the core, and into the receiver crystal. The received electrical signal is then amplified and filtered through the receiving section of the pulser-receiver and displayed on a digital storage oscilloscope. The signals are high pass filtered above 0.3 MHz to eliminate low frequency noise. The time series displayed on the oscilloscope is then digitized and transferred to a computer for subsequent analysis including picking the first arrival of the compressional and shear wave energy to compute the compressional and shear wave velocities. The accuracy of the travel time is ± 0.02 microseconds.

A diagram of the system is shown in Figure 4. Pneumatic actuators couple the transducer assemblies in both the axial and radial directions. The stress across the interface for both the matched transducer pairs is identical; this is accomplished by adjusting the loading areas in the pneumatic actuators. The titanium pieces for the radial transducers are concave to mate with the rock surface. Because of the geometry of the interface, only polarizations parallel to the core axis are propagated for shear waves in the radial direction.

2.3.1 Detailed Procedure for Compressional and Shear Wave Velocity Measurements

The detailed procedure for measuring compressional and shear wave velocities on room dry and water saturated tuff specimens is presented below.

1. Grind the tuff specimen to a right circular cylinder with a nominal length to diameter ratio of 2:1. The sample is machined to meet or exceed the tolerances specified in SNL TP-51. For the saturated condition, a thin cellophane wrap is place around the specimen to maintain its moisture content during the measurements.

2. Coat the ends of the specimen with a shear wave couplant. Shear wave couplant is a viscous substance that facilitates the propagation of shear waves across the specimen-titanium interface. Shear wave couplant is also applied at the midpoint of the specimen where the velocities normal to the specimen axis are measured.

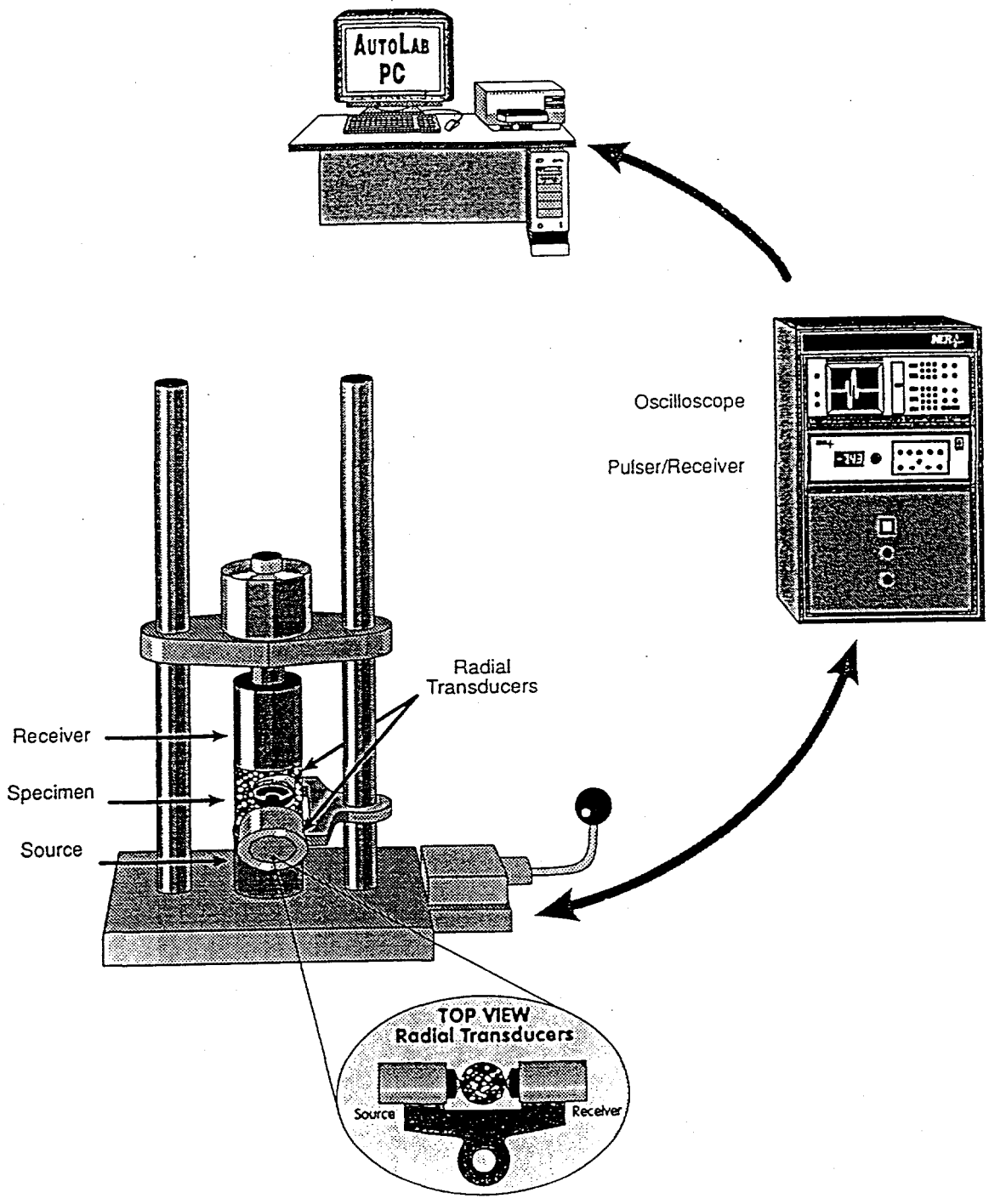

Figure 4: Schematic of the apparatus used to measure ultrasonic velocities parallel and normal to the core axis under ambient conditions prior to testing in unconfined compression.

3. Position the specimen in the ultrasonic velocity measuring apparatus. Ensure that the specimen is lined up with the transducers in the axial direction.

4. Increase the pressure in the pneumatic actuators to press the axial and radial transducer assemblies against the specimen. Ensure that the specimen has not shifted during this procedure and that the specimen is well coupled to the transducer assembly.

5. Turn on the data acquisition system. First, set the signal selection switch for a compressional (P) wave along the axis of the specimen. Observe the received signal on the digital oscilloscope. Adjust the pulse excitation signal gain and/or attenuation to obtain a well-defined signal.

6. Initiate the data acquisition software to store the waveform; capture and store the waveform.

7. Capture the two shear (S1 and S2) wave polarizations with a propagation direction parallel to the core axis, and the compressional and shear wave signals for the propagation direction normal to the core axis, following the same procedure used for the compressional wave in steps 5 and 6.

8. Compute the compressional and shear wave velocities by determining the travel time through the specimen and dividing it into the sample length. The travel time is determined by picking the time of the first arrival of the compressional or shear wave energy. The measured travel times are reduced by the travel time through the titanium substrates. The corrected travel time is then divided into the sample length to determine the velocity.

9. Print the stored waveforms, along with the computed compressional and shear wave velocities, and place the data in the scientific notebook.

10. Compute the dynamic Young's modulus (E) and Poisson's ratio (ν) from the velocity data collected parallel to the core axis and the bulk density of the specimen for the measurement condition. The dynamic elastic moduli are computed as follows:

$$E = [\rho V_s^2 (3V_p^2 - 4V_s^2)/(V_p^2 - V_s^2)]$$

$$\nu = (V_p^2 - 2V_s^2)/[2(V_p^2 - V_s^2)]$$

where

V_p = compressional wave velocity, km s^{-1}

V_s = average shear wave velocity, km s^{-1}

ρ = bulk density for the measurement conditions, g cm^{-3}

2.4 Confined Compression to Failure

The confined compression experiments were performed on saturated right-circular cylinders of tuff with a nominal length to diameter ratio of 2:1, at a constant axial strain rate of 10^{-5} s^{-1} at room temperature. System checks of the entire test system were conducted during this experimental series in order to establish the performance of the system using an aluminum specimen with the same nominal dimensions as the tuff test specimens.

A description of the equipment and an overview of the test procedures places the step-by-step procedures in the proper context. All the compression tests were carried out in a servo-controlled hydraulic loading frame with a capacity of 1.4×10^6 N. The servo-controller is a self-contained digital unit, which operates in either force or displacement feedback. The rate at which the reference signal is updated can be varied from 10^{-5} to 10^3 times per second. The loading rate or displacement rate depends on the range of the feedback transducers and the time between steps. The feedback transducers are conditioned with amplifiers in the servo-control unit and balanced so that the full-scale output of the transducer corresponds to the maximum range of the reference signal generator. The full scale output (10 V) is divided into 2^{12} discrete steps.

Figure 5 is a schematic diagram of an instrumented specimen. The test assembly consists of the specimen positioned between hardened steel end caps. The specimen is jacketed with 0.13 mm thick copper.

For this experimental series, outputs from six transducers were monitored. The output from each device is conditioned, amplified, converted to digital format, and recorded as a function of time. The outputs from the devices were recorded with a microcomputer acquisition system. Each channel is sampled at a frequency of 4 Hz.

For constant strain rate tests the loading frame is operated in displacement feedback mode. The displacement can be controlled to within $\pm 10^{-3}$ mm. The accuracy and the reproducibility of the strain rate is $\pm$ 0.5 percent.

During each test the axial and radial displacements of the specimen were measured with Linear Variable Differential Transformers (LVDTs). A schematic of their arrangement is shown in

Axial and Radial Deformation Instrumentation

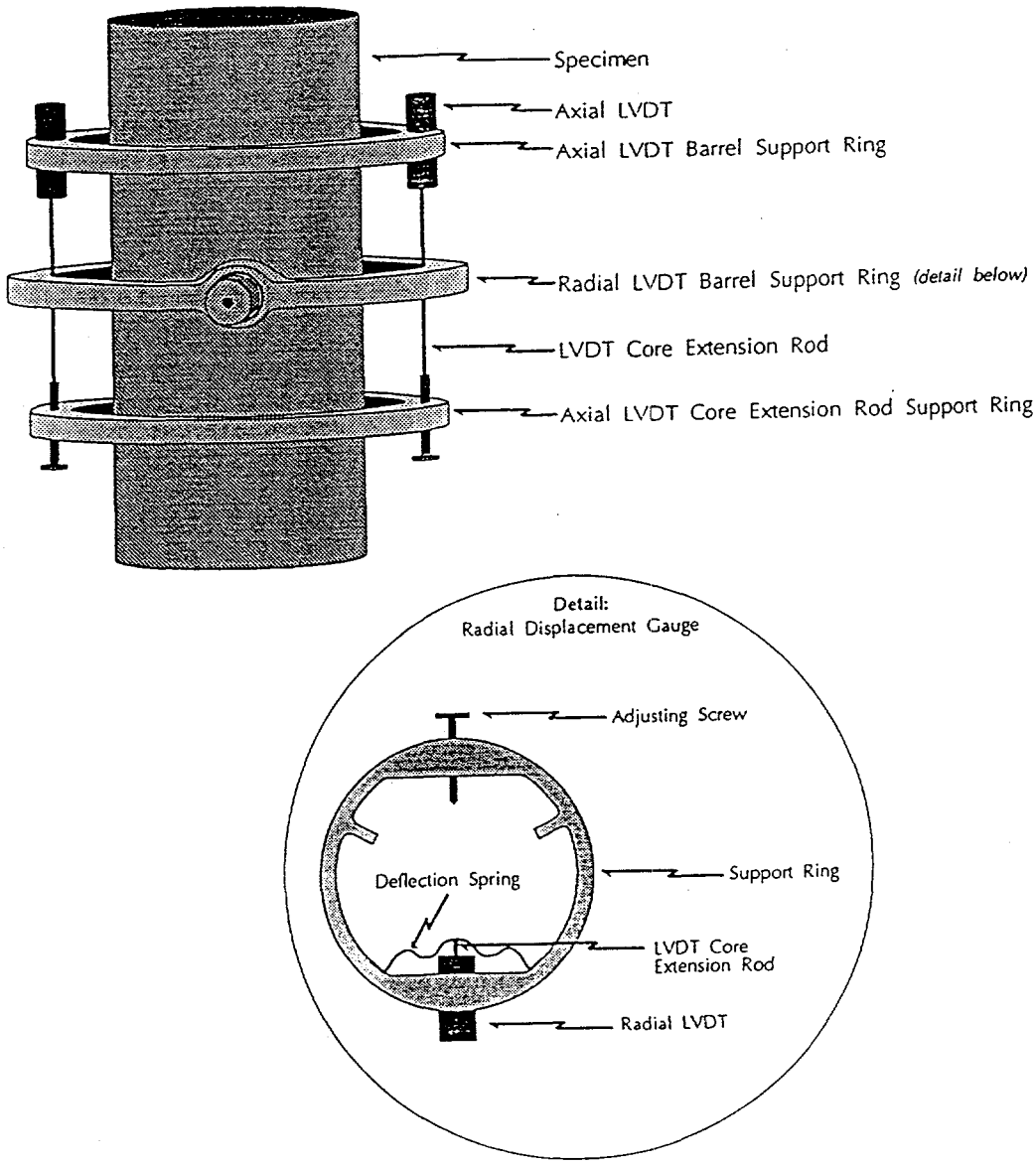

Figure 5: Schematic of the transducer configuration used to measure the axial and radial displacement of specimens during unconfined and confined compression tests.

Figure 5. Two LVDTs monitor the axial displacement. The LVDT barrels are secured in a ring which is attached one specimen radius from the upper end of the specimen. The cores for the displacement transducers are on extended rods which attach to a second ring separated from the first by one specimen diameter. The second ring is mounted approximately one specimen radius from the lower end of the specimen.

A direct way to measure radial strain is with the radial displacement gage developed by Holcomb and McNamee (1984). Their gage consists of an LVDT mounted in a ring which is spring loaded against the surface of the specimen (Figure 5). The core of the LVDT is connected to the spring. As the specimen diameter changes, the spring deflects, changing the position of the core within the barrel of the LVDT in direct proportion to the radial displacement.

The force on the test column is measured with a load cell. The accuracy of the load cell is better than 0.5 percent of its full-scale output; the combined linearity and hysteresis are better than 1.0 percent. The position of the hydraulic piston is observed with a displacement transducer. This transducer provides feedback control in constant strain rate tests and is continuously monitored along with all the transducer outputs. The hydraulic piston advances at a constant rate; this is equivalent to deforming the specimen at a constant strain rate only in the linear portion of the stress-strain curve.

The confining pressure was measured with a pressure transducer. The accuracy of the device is 1% of the full scale output (35 MPa).

Checks of the entire test system are made using a sample of 6061-T6511 aluminum with the same nominal dimensions as the test specimens. One check is performed before the experiments on a suite of tuff samples, and then after each group of ten tuff samples. Each check was performed in unconfined compression at a nominal strain rate of 10^{-5} s^{-1}, at ambient temperature. The system is determined to be operating properly when the elastic properties measured for the aluminum are within ±5% of its published values.

2.4.1 Experimental Procedures For Confined Compression Tests

Specimens of tuff were tested to failure at a constant strain rate of 10^{-5} s^{-1}, at confining pressures of 5 and 10 MPa, and at ambient temperature. The following sections include the step-by-step procedures for the confined compression tests. The procedure was based on TP-219 "Unconfined Compression Experiments at 22 °C and a Strain Rate of 10^{-5} s^{-1}" and conforms to ISRM "Suggested Methods for Determining the Strength of Rock Materials in Triaxial Compression" and ASTM D 2664 "Triaxial Compressive Strength of Undrained Rock Core Specimens Without Pore Pressure Measurements."

1. Each tuff specimen is machined according to SNL TP-51, and saturated according to SNL TP-64. Velocity measurements are performed before, and after the saturation procedure.

2. List all transducers used for each experiment. The information includes the serial numbers of the device, signal conditioning amplifier number, the computer channel on which the output is recorded, and the scaling factor for the amplified output.

3. Visually inspect the test specimen and note any surface irregularities and imperfections.

4. Jacket the saturated specimen in 0.13 thick copper foil. The copper is extended 12 mm beyond each end of the specimen. Hardened steel end caps are then positioned at each end of the specimen.

5. The jacket is sealed.

6. The sample assembly is pressurized to 10 MPa to seat the jacket. Once the jacket is seated it is visually inspected to ensure that there are no holes to allow invasion of the confining medium into the specimen.

7. Position the ring supporting the two axial LVDT barrels approximately one specimen radius from the upper end of the specimen. Carefully center the ring so that it is concentric with the specimen.

8. Position the LVDT ring used to measure the radial displacement at the midpoint of the specimen. The supporting ring for the LVDT (with a range of $\pm$ 1.25 mm) is positioned in such a way to ensure that the line between the adjusting screw on the ring and the axis of the core barrel of the LVDT passes through the axis of the specimen and is perpendicular to the axis of the specimen.

9. Position the lower support ring for the axial LVDT concentrically about the specimen approximately one specimen diameter from the upper ring. This ring supports the stainless steel extension rods for the LVDT cores. Ensure that the axes of the LVDT core barrels are aligned parallel with the axis of the specimen. The extension rods are supported with adjusting screws that are secured with locking nuts.

10. Measure the center-to-center separation of the axial LVDT support rings with a caliper-micrometer. Record this value in the scientific notebook.

11. Place the specimen assembly on the base plug of the pressure vessel in the load frame.

12. Connect the two axial LVDTs and the radial LVDT to the electrical leads in the base plug.

13. Make the final mechanical adjustments on the LVDTs. Each LVDT is adjusted so that its initial amplified output is approximately 0.10 V. Note that all the LVDTs are wired so that increasing the specimen diameter and shortening the specimen assembly results in an increasing positive output voltage.

14. Load the sample assembly and base plug into the pressure vessel.

15. Advance the loading piston, in displacement control, until a small load is exerted on the specimen column (just enough to hold the specimen securely in position).

16. Increase the confining pressure to 5 or 10 MPa. Argon is used as a confining medium.

17. Allow 10 minutes for the system to achieve thermal equilibrium and check for leaks.

18. Retract the hydraulic piston until there is no differential stress on the specimen.

19. Initiate data acquisition. The amplified outputs from six transducers are monitored and recorded using a microprocessor-based data acquisition system. The transducers that are monitored include the three LVDTs, the feedback displacement transducer, the force cell and the confining pressure transducer. All the channels are sampled every 0.25 seconds. Data is stored when the output of one channel deviates from the previous value by a preselected threshold. The threshold for each channel is independently set prior to the experiment.

20. Adjust the setting on the displacement rate controller to the displacement rate that corresponds to a nominal strain rate of 10^{-5} s^{-1}. After a final check of all the transducer values, start loading the specimen.

21. Load the specimen to failure.

22. Release the confining pressure, remove the specimen from the pressure vessel, and examine the mode of failure. Record the observations in the scientific notebook. Dry the specimen according to TP-65. Photograph the specimen. Ensure that the field of view of the photograph includes the specimen identification, TP identification, scale, date, type of test performed, and NER identification.

23. Return the specimen to its original container, and return it to storage.

24. Reduce the data. The following elastic constants are computed:

(a) Young's modulus, E
$E = \Delta$ (axial stress) / Δ (axial strain)

(b) Poisson's ratio, ν
$\nu = \Delta$ (radial strain) / Δ (axial strain)

The elastic constants are computed by performing a least-squares linear fit to the data collected between 10 and 50 percent of the stress difference at failure. Stress difference is computed by dividing the axial force difference by the initial cross sectional area of the specimen. Stress is reported in MPa. Axial strain is obtained by dividing the average axial displacement of the axial LVDT support rings by the original ring separation distance. Radial strain is computed by dividing the change in radial displacement observed by the radial LVDT by the initial specimen diameter. All strains are reported in millistrain.

3.0 RESULTS

The results of the bulk properties measurements and the confined compression experiments are presented in Tables 1, 2, 3, 4, and 5. Tables 1 and 4 present the data associated with the confined compression tests. The data include dry bulk density, saturated bulk density, average grain density, porosity, compressional and shear wave velocities for the room dry and water saturated conditions, both parallel [axial] and normal [radial] to the core axis, confining pressure, static Young's modulus, static Poisson's ratio, differential axial stress at failure, and axial strain at failure. These data have been grouped according to depth. The thermal/mechanical unit and lithostritagraphic unit are indicated for each specimen. For some specimens, reliable compressional and shear wave velocities were not obtained due to poor signal quality. The absence of the data is reflected in Tables 1 and 4.

The porosity via grain density reported in Tables 1, 3, 4, and 5 is the total porosity including occluded porosity. The value is computed from the grain density and dry bulk density. The total porosity is most applicable when elastic constants and strength characteristics are measured. The porosity computed from the dry and saturated bulk densities is typically lower than the total porosity and reflects the interconnected porosity. The latter value is applicable when considering fluid transport properties.

TABLE 1

SUMMARY DATA SHEET: NRG-6 BOREHOLE

Confined Compression Tests: 50.8 mm Diameter Specimens

Sample IDs are shortened from the "NRG-6-Depth-SNL-Subdivision" Format
Test Conditions: Saturated samples, ambient temperature, and a nominal strain rate of 10E-5 sE-1.

Sample ID:	5.7-A	46.4-A	122.7-A	290.5-A	326.0-A	362.0-A	394.6-A					
T/M Unit:	TCw	TCw	TCw	TSw1	TSw1	TSw1	TSw1					
Lithostratigraphy:	Tpcpll	Tpcpll	Tpcpln	Tptrn	Tptrn	Tptrn	Tptrn					
Porosity via Saturation (%):	8.6	7.6	14.4	11.1	14.2	14.1	10.5					
Porosity via Grain Density (%):	10.4	8.4	16.1	12.9	15.5	16.6	12.4					
Dry Bulk Density (g/cc):	2.239	2.287	2.096	2.218	2.188	2.147	2.244					
Saturated Bulk Density (g/cc):	2.325	2.362	2.240	2.329	2.330	2.288	2.349					
Sat. P Velocity at 0 MPa (km/s):	4.620	4.522	3.773	4.325	4.069	N/A*	4.145					
Sat. S1 Velocity at 0 MPa (km/s):	2.588	N/A*	N/A*	N/A*	N/A*	N/A*	N/A*					
Sat. S2 Velocity at 0 MPa (km/s):	2.598	N/A*	N/A*	N/A*	N/A*	N/A*	N/A*					
Confining Pressure (MPa):	5	10	10	10	5	10	5					
Static Young's modulus (GPa):	24.4	22.3	18.8	28.4	25.4	17.5	20.0					
Static Poisson's ratio:	0.07	0.10	0.17	0.21	0.22	0.19	0.20					
Ultimate Diff. Axial Stress (MPa):	120.3	147.9	173.1	218.5	111.1	83.6	94.3					
Ax. Strn at Ult. Ax. Sts. (milstrn):	5.51	8.99	8.70	8.03	4.91	7.29	6.71					

P is the compressional wave, S1 and S2 are the two orthogonally polarized shear waves.
Elastic properties are calculated between 10 and 50% of the ultimate differential axial stress.

*: Signal quality too poor for meaningful velocity measurements.

TABLE 2

SUMMARY DATA SHEET: NRG-6 BOREHOLE

(Pressure Effects)

Average Grain Density Tests

Sample IDs are shortened from the "NRG-6-Depth-SNL-Subdivision" Format

Group:	Triax	Triax	Triax	Triax	Triax	Triax	Triax	Triax	Triax	Triax
Sample ID:	5.7-B	46.4-B	81.8-B	122.7-B	172.6-B	221.0-B	290.5-B	326.0-B	362.0-B	394.6-B
T/M Unit:	TCw	TCw	TCw	TCw	PTn	PTn	TSw1	TSw1	TSw1	TSw1
Lithostratigraphy:	Tpcpll	Tpcpll	Tpcpln	Tpcpln	Tpbt3	Tpbt2	Tptrn	Tptrn	Tptrn	Tptrn
Grain Density (g/cc):	2.500	2.495	2.503	2.498	2.460	2.405	2.547	2.591	2.576	2.560

Group:	Triax	Triax	Triax	Triax	Triax	Triax	Triax	Triax	Triax	Triax
Sample ID:	429.0-B	525.0-B	558.9-B	599.6-B	642.7-B	777.2-B	791.6-B	1008.8-B	1062.9-B	1080.3-B
T/M Unit:	TSw1	TSw1	TSw1	TSw1	TSw1	TSw2	TSw2	TSw2	TSw2	TSw2
Lithostratigraphy:	Tptrl	Tptpul	Tptpul	Tptpul	Tptpul	Tptpmn	Tptpmn	Tptpll	Tptpll	Tptpll
Grain Density (g/cc):	2.533	2.503	2.519	2.534	2.550	2.502	2.519	2.586	2.554	2.541

Group:	Triax
Sample ID:	1092.3-B
T/M Unit:	TSw2
Lithostratigraphy:	Tptpll
Grain Density (g/cc):	2.547

TABLE 3

SUMMARY DATA SHEET: NRG-6 BOREHOLE

Confined Compression Tests: 50.8 mm Diameter Specimens
Porosity Values for Untestable Sample Intervals

Sample IDs are shortened from the "NRG-6-Depth-SNL-Subdivision" Format

Sample ID:	81.8-A	172.6-A	221.0-A	429.0-A	525.0-A	558.9-A	599.6-A	642.7-A	777.2-A	791.6-A
T/M Unit:	TCw	PTn	PTn	TSw1	TSw1	TSw1	TSw1	TSw1	TSw2	TSw2
Lithostratigraphy:	Tpcpln	Tpbt3	Tpbt2	Tptrl	Tptpul	Tptpul	Tptpul	Tptpul	Tptpmn	Tptpmn
Porosity via Grain Density (%):	6.2	50.9	43.3	18.1	26.3	28.2	30.2	18.7	8.0	11.4

Sample ID:	1008.8-A	1062.9-A	1080.3-A	1092.3-A						
T/M Unit:	TSw2	TSw2	TSw2	TSw2						
Lithostratigraphy:	Tptpll	Tptpll	Tptpll	Tptpll						
Porosity via Grain Density (%):	13.2	22.6	18.1	11.7						

TABLE 4

SUMMARY DATA SHEET: NRG-7/7A BOREHOLE

Confined Compression Tests: 50.8 mm Diameter Specimens

Sample IDs are shortened from the "NRG-7-Depth-SNL-Subdivision" Format
Test Conditions: Saturated samples, ambient temperature, and a nominal strain rate of 10E-5 sE-1.

Sample ID:	345.0-A	411.4-A	427.6-A	441.0-A	454.6-A	470.2-A	483.3-A	671.4-A	672.0-A	717.7-A	805.6-A	827.4-A
T/M Unit:	TSw1	TSw1	TSw1	TSw1	TSw1	TSw1	TSw1	TSw1	TSw1	TSw1	TSw2	TSw2
Lithostratigraphy:	Tptrn	Tptrn	Tptrn	Tptrn	Tptrn	Tptrn	Tptrl	Tptpul	Tptpul	Tptpul	Tptpmn	Tptpmn
Porosity via Saturation (%):	12.6	14.9	12.5	13.1	13.0	9.9	13.0	12.2	11.8	15.0	11.7	13.6
Porosity via Grain Density (%):	15.0	16.5	14.3	14.4	14.1	11.1	14.9	14.3	12.7	16.7	12.6	14.6
Dry Bulk Density (g/cc):	2.142	2.151	2.209	2.199	2.197	2.268	2.166	2.176	2.217	2.130	2.212	2.178
Saturated Bulk Density (g/cc):	2.268	2.300	2.334	2.330	2.327	2.367	2.296	2.297	2.335	2.280	2.330	2.314
Sat. P Velocity at 0 MPa (km/s):	4.371	N/A*	N/A*	N/A*	N/A*	N/A*	N/A*	N/A*	N/A*	N/A*	N/A*	N/A*
Sat. S1 Velocity at 0 MPa (km/s):	N/A*	N/A*	N/A*	N/A*	N/A*	N/A*	N/A*	N/A*	N/A*	N/A*	N/A*	N/A*
Sat. S2 Velocity at 0 MPa (km/s):	N/A*	N/A*	N/A*	N/A*	N/A*	N/A*	N/A*	N/A*	N/A*	N/A*	N/A*	N/A*
Confining Pressure (MPa):	5	10	5	10	5	10	5	5	10	5	10	10
Static Young's modulus (GPa):	29.0	17.8	16.1	20.3	14.0	19.8	14.4	32.4	22.3	17.8	21.4	23.4
Static Poisson's ratio:	0.24	0.20	0.14	0.22	0.24	0.33	0.28	0.19	0.11	0.42	0.27	0.33
Ultimate Diff. Axial Stress (MPa):	99.5	78.4	68.1	93.3	65.5	129.3	62.1	106.9	217.9	71.9	137.1	125.3
Ax. Strn at Ult. Ax. Sts. (milstrn):	3.97	4.72	9.04	7.96	9.39	8.37	5.95	3.96	9.26	5.99	5.05	6.46

P is the compressional wave, S1 and S2 are the two orthogonally polarized shear waves.
Elastic properties are calculated between 10 and 50% of the ultimate differential axial stress.

*: Signal quality too poor for meaningful velocity measurements.

TABLE 4 (Continued)

SUMMARY DATA SHEET: NRG-7/7A BOREHOLE

Confined Compression Tests: 50.8 mm Diameter Specimens

Sample IDs are shortened from the "NRG-7-Depth-SNL-Subdivision" Format
Test Conditions: Saturated samples, ambient temperature, and a nominal strain rate of 10E-5 sE-1.

Sample ID:	861.7-A	977.8-A	1399.1-A	1400.5-B								
T/M Unit:	TSw2	TSw2	TSw2	TSw2								
Lithostratigraphy:	Tptpmn	Tptpll	Tptpln	Tptpln								
Porosity via Saturation (%):	9.4	11.8	7.2	5.8								
Porosity via Grain Density (%):	9.6	12.7	6.9	5.7								
Dry Bulk Density (g/cc):	2.284	2.251	2.337	2.371								
Saturated Bulk Density (g/cc):	2.378	2.369	2.409	2.428								
Sat. P Velocity at 0 MPa (km/s):	N/A*	N/A*	N/A*	N/A*								
Sat. S1 Velocity at 0 MPa (km/s):	N/A*	N/A*	N/A*	N/A*								
Sat. S2 Velocity at 0 MPa (km/s):	N/A*	N/A*	N/A*	N/A*								
Confining Pressure (MPa):	5	10	5	10								
Static Young's modulus (GPa):	33.9	29.6	30.8	39.6								
Static Poisson's ratio:	0.21	0.20	0.22	0.26								
Ultimate Diff. Axial Stress (MPa):	245.8	206.9	147.6	251.8								
Ax. Strn at Ult. Ax. Sts. (milstrn):	8.83	8.50	5.43	8.05								

P is the compressional wave, S1 and S2 are the two orthogonally polarized shear waves.
Elastic properties are calculated between 10 and 50% of the ultimate differential axial stress.

*: Signal quality too poor for meaningful velocity measurements.

Table 5

SUMMARY DATA SHEET: NRG-7/7A BOREHOLE

Confined Compression Tests: 50.8 mm Diameter Specimens
Porosity Values for Untestable Sample Intervals

Sample IDs are shortened from the "NRG-7-Depth-SNL-Subdivision" Format

Sample ID:	655.7-A	1362.8-A								
T/M Unit:	TSw1	TSw2								
Lithostratigraphy:	Tptpul	Tptpln								
Porosity via Grain Density (%):	20.7	9.4								

Tables 3, and 5 list the specimens for which only average grain density, dry bulk density, and porosity were measured. The thermal/mechanical unit and the lithostratagraphic unit for each of these specimens are indicated.

All specimens tested in this study were ideally water saturated. However, the saturation is not 100%. Porosities computed using the saturated bulk density and dry bulk density yield consistently lower values than those computed using the average grain density and dry bulk density. In part, the differences can be attributed to an under-estimation of the saturated bulk density due to water loss on the surface of the specimen. However, these errors are small and cannot account for the total discrepancy. The major contribution to the differences is occluded porosity (isolated pores that are not filled during saturation). As a result, the specimens are not 100% saturated prior to mechanical testing; the saturations range between 80 and 95%.

3.1 Confined Compression to Failure

Confined compression experiments were carried out on twenty three specimens; seven specimens were from the USW NRG-6 borehole and sixteen were from the USW NRG-7/7A borehole. Three specimens from the TCw (Tpcpll-Tpcpln), fourteen from the TSw1 (Tptrn-Tptpul) and six from the TSw2 (Tptpmn-Tptpln) thermal/mechanical units were tested. Specimens were selected from limited core remaining from these boreholes after the unconfined, Brazil, etc. test specimens were chosen and tested. Stress-strain plots for all of the tests are shown in Appendix I.

The specimens typically failed in a brittle fashion, with a rapid increase in diametric strain very near failure, and an immediate decrease in axial stress when the maximum load had been applied. The plots shown in Appendix I present data up to the maximum stress, as there are typically few data points collected post-failure due to the catastrophic nature of the failure. Figure 6 presents plots for a typical experiment on a TSw2 (Tptpll) specimen that show slight acceleration in the strains as the maximum stress is approached. There is an immediate loss of strength as the maximum stress is reached. Radial, and volumetric strain as a function of differential stress are linear up to approximately 80% of the maximum differential stress. Dilation, or the initiation of extension cracks, is mostly limited to the near failure regime. Sharp, straight extension fractures concentrated at the specimen midpoint, generally developing parallel to the specimen axis are typical for the nonlithopysal specimens. The failure of the highly lithophysal specimens (TSw1) is also dominated by extension fractures, but axial compaction of the lithophysal cavities and their associated vapor-phase alteration zones, and the collapse of the welded matrix around them constitute much of the deformation in them as well. Shear fractures typically do not develop, as

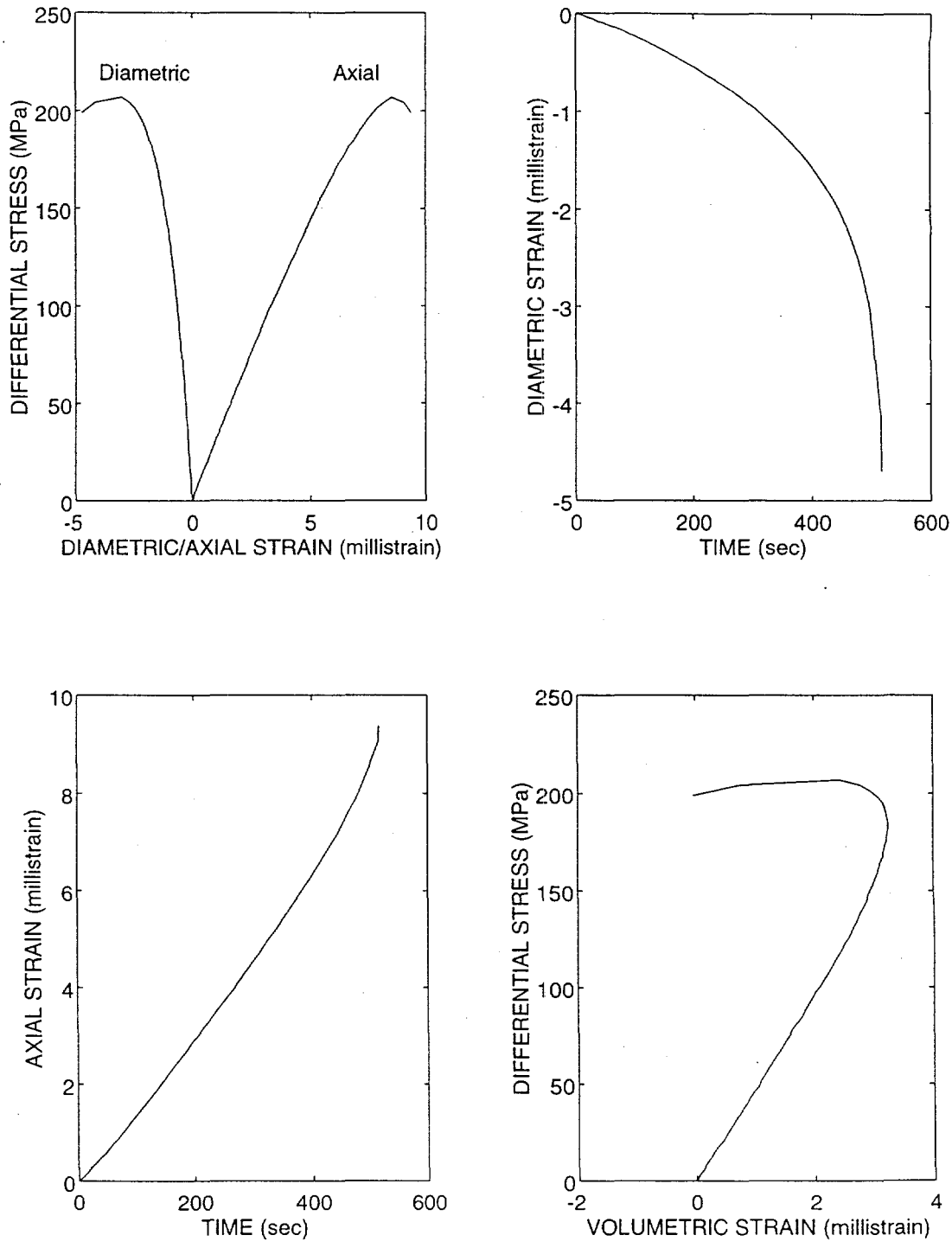

Figure 6. Data plots for a confined compression test on welded tuff at a confining pressure of 10 MPa. The TSw2 (Tptpll) specimen is from the USW NRG 7/7A borehole, and was collected at a depth of 977.8 feet (298.0 meters).

the extension fractures dominate. The extent of the fractures is controlled by heterogeneities (e.g., lithophysae or vapor-phase alteration zones). The fractures often originate, or terminate at the heterogeneities.

Because of the heterogeneous nature of the tuffs at Yucca Mountain, the size and distribution of the test specimen population is not sufficient to quantify the effect of pressure on strength and elastic constants. The properties are influenced by many factors, including mineralogy, welding, heterogeneities (e.g., lithophysae, fractures, and vapor-phase alteration zones), and particularly the abundance and distribution of pore spaces. Price and Bauer (1985) have shown that there is a strong correlation between porosity and fracture strength for unconfined compression tests on a wide range of tuffs from the vicinity of Yucca Mountain. More recent studies (Martin et al., 1994, and Martin et al., 1995) have also observed a first order effect of porosity on the strength of tuff in unconfined compression for specimens from the USW NRG-6 and USW NRG-7/7A boreholes. Figures 7 and 8 are plots of stress difference at failure and Young's modulus as a function of porosity for the specimens tested in confined compression. It is clear that there is a consistent decrease in these properties as porosity increases. Obviously, parameters other than confining pressure have an effect on the mechanical properties and make an analysis of the pressure effects very difficult.

The summary presented in Table 6 indicates the difficulty in evaluating the effects of pressure on the mechanical properties of tuff. When the data is segregated by thermal/mechanical unit, and further by including the large effect porosity has on tuff strength, it becomes obvious that it is difficult to develop a believable pressure effect model for the entire interval. An analysis of these results show the limited specimen population and the uneven distribution of test specimens throughout the stratigraphic column. Suitable test specimens from the TSw2 unit were particularly sparse.

The data for the TSw1 unit show the anticipated dependence of strength on confining pressure. This is true even though this unit is highly heterogeneous. Stress difference at failure increased from 61.7 to 84.9 MPa (38%) as the confining pressure increased from 0 to 5 MPa, and from 84.9 to 136.8 MPa (61%) as the confining pressure increased from 5 to 10 MPa. Because the average porosities of these TSw1 specimens are very similar, the effect of porosity variations can be assumed to be minimal. In spite of the increase in strength, Young's modulus does not vary with confining pressure for these specimens.

The data for the TSw2 unit was collected on a limited number of specimens (two at 5 MPa, and four at 10 MPa). This unit has the highest average strengths, at both elevated confining pressures, of the three units tested. The data do not however show an increase in strength with increasing confining pressure. In fact, a decrease in strength is observed between 5 and 10 MPa.

Table 6

USW NRG-6 and USW NRG-7/7A Pressure Effects Summary

Thermal/Mechanical Unit:	TCw (# Tested)	TSw1 (# Tested)	TSw2 (# Tested)	TSw1/TSw2 Only (# Tested)
Average Strength at 0 MPa (MPa):	186.3 (11)	61.7 (35)	151.1 (26)	99.8 (61)
Average Young's Modulus at 0 MPa (GPa):	29.9	20.0	32.2	25.1
Average Porosity (%):	8.9	14.5	10.9	13.0
Average Strength at 5 MPa (MPa):	120.3 (1)	84.9 (8)	196.7 (2)	107.3 (10)
Average Young's Modulus at 5 MPa (GPa):	24.4	21.1	32.4	23.4
Average Porosity (%):	10.4	14.7	8.3	13.4
Average Strength at 10 MPa (MPa):	160.5 (2)	136.8 (6)	180.3 (4)	154.2 (10)
Average Young's Modulus at 10 MPa (GPa):	20.6	21.0	28.5	24.0
Average Porosity (%):	12.3	14.0	11.4	13.0

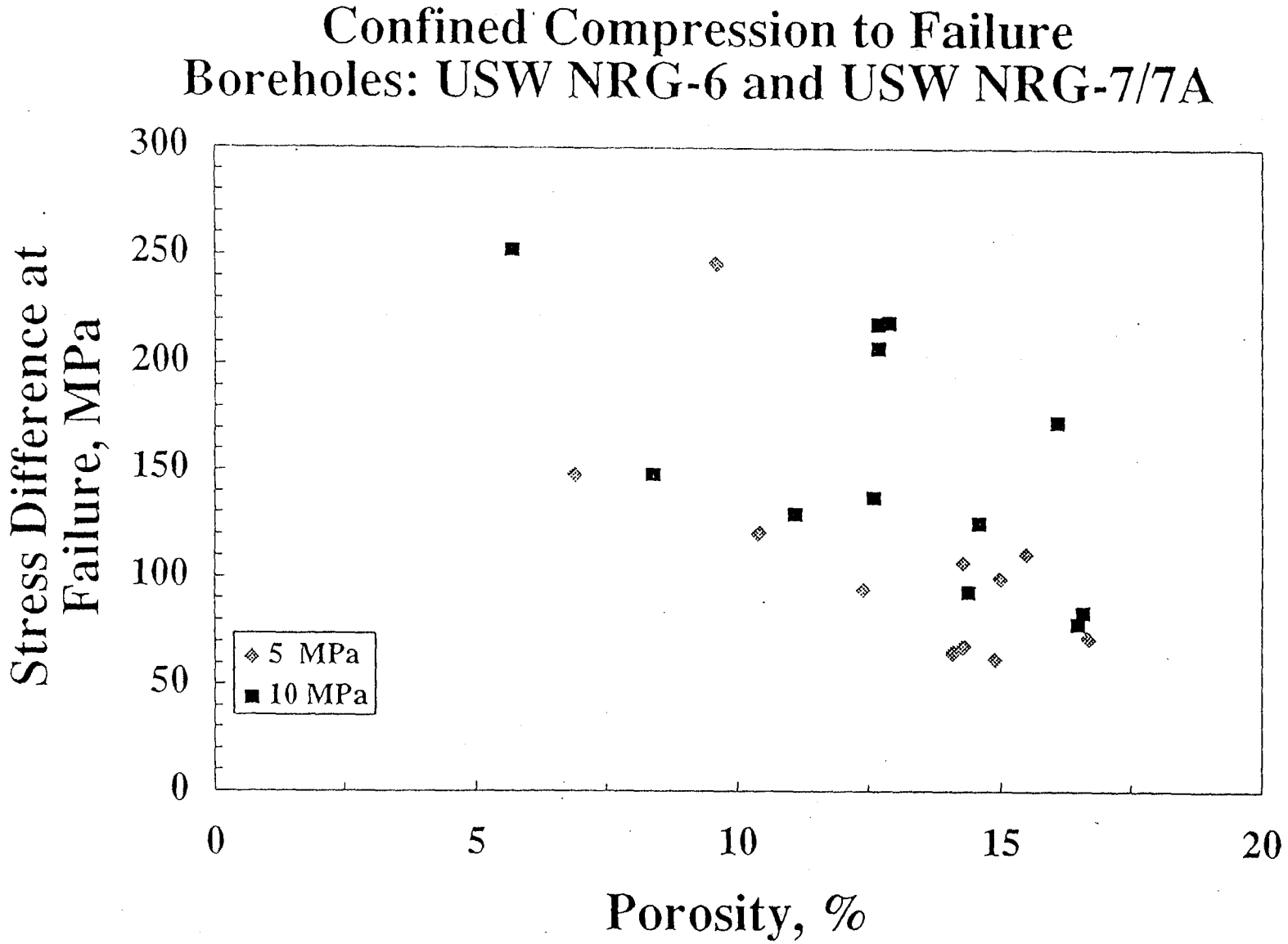

Figure 7: Stress difference at failure is shown as a function of porosity.

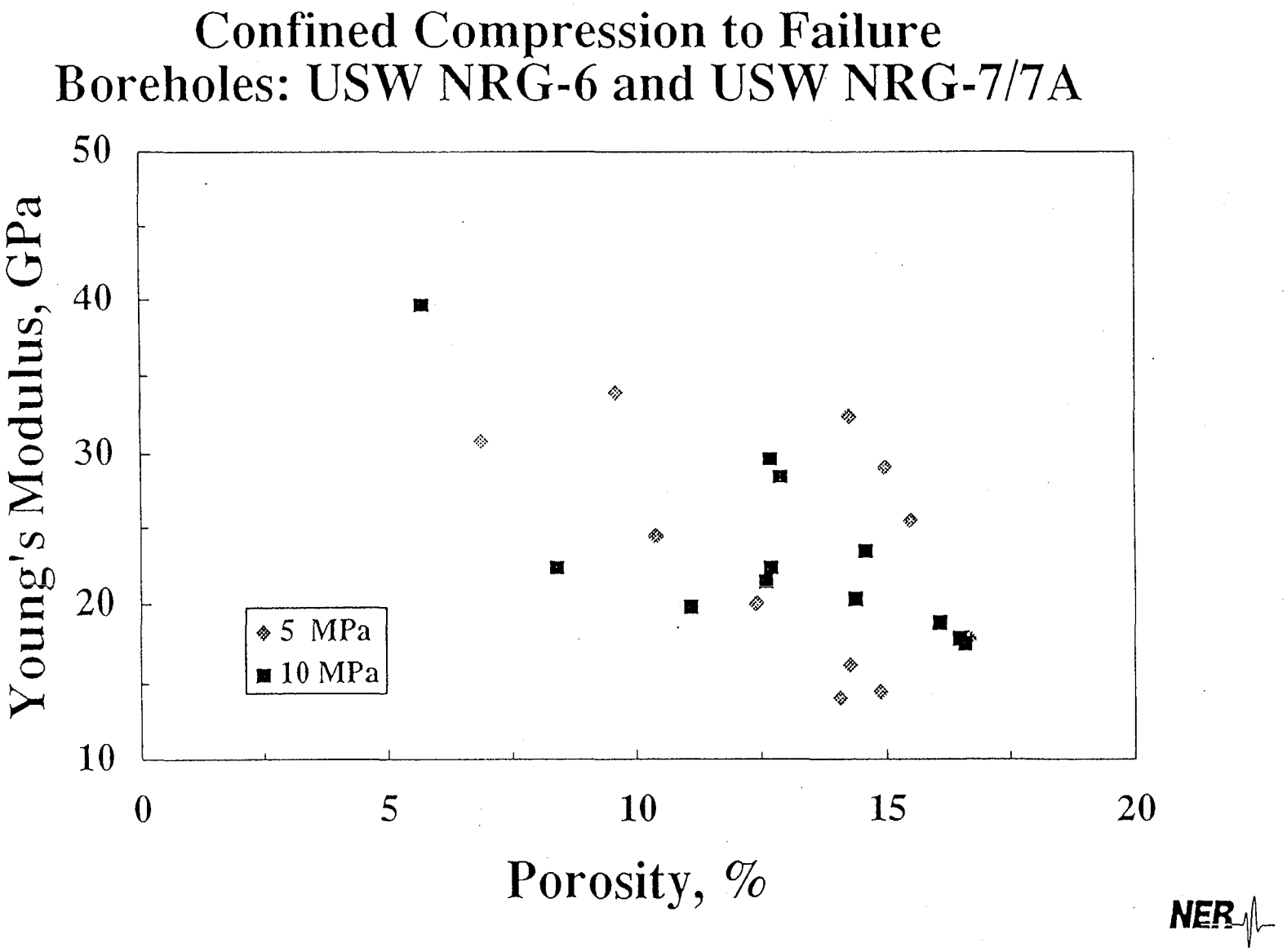

Figure 8: Young's modulus is shown as a function of porosity.

The data suggest strength is more strongly affected by the porosity than the confining pressure. Because there is insufficient data from the TSw2 unit, a definitive relationship between strength and confining pressure is not possible. Again, the Young's modulus data does not show a dependence on confining pressure.

Only three specimens of the TCw unit from the USW NRG-6 borehole were suitable for testing in confined compression. None were chosen from the USW NRG-7/7A borehole. No quantitative analysis can be carried out with this very limited population.

Other than their relative abundance of heterogeneities, the TSw1 and TSw2 units are lithologically very similar. The matrices of these units have a particularly consistent character. The results for these two units alone indicate an expected pressure effect. The magnitude of the effect is indiscernible, due to the limited specimen population, but the trend is consistent with what is expected. Note that the average porosities are again very similar in this group. No pressure effect on Young's modulus is expressed in these data.

The data does indicate that increased confining pressure has the effect of increasing the strength of tuff in laboratory confined compression testing. Figure 9 is a plot of the stress difference at failure as a function of confining pressure. This figure illustrates the scatter in the strengths at any condition, and the general trend of greater strength with increasing confining pressure. The magnitude of the effect, either for the entire tuff interval, or for individual units is difficult to interpret.

No pressure effect on Young's modulus has been identified; this is consistent with earlier studies that show the elastic constants for welded tuff are independent of confining pressure. For example, linear compressibility on TSw2 exhibits a very small pressure dependence up to 50 MPa (Martin et al., 1992). Similarly, compressional and shear wave velocities, also on welded tuff, appear unaffected by pressures to 25 MPa (Martin et al., 1992; Price et al., 1994).

Because the laboratory mechanical properties data for the tuff is so variable, and dependent on a number of factors, a quantitative characterization of the effects of confining pressure requires a large number of tests. General conclusions may be presented, but it is not possible to precisely define the behavior of the tuff as a function of confining pressure with the available data.

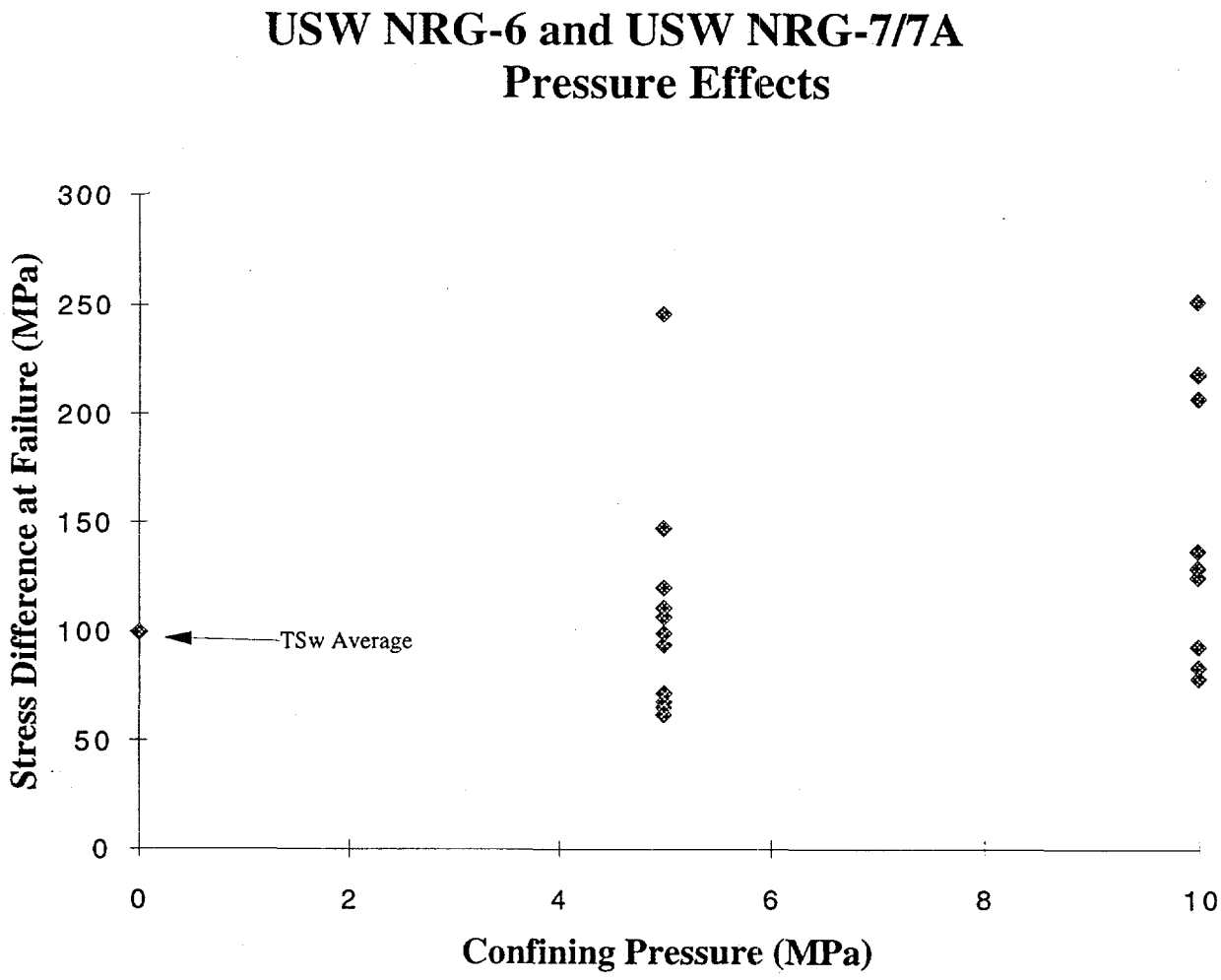

Figure 9. Plot of differential axial stress at failure as a function of confining pressure for welded tuff from the USW NRG-6 and USW NRG-7/7A boreholes.

4.0 REFERENCES

ASTM, 1986, Standard Test Method for Triaxial Compressive Strength of Undrained Rock Core Specimens Without Pore Pressure Measurements, ASTM D 2664-86, American Society for Testing and Materials, Philadelphia, PA.

Boyd, P.J, R.J. Martin III, and R.H. Price, 1994, An Experimental Comparison of Laboratory Techniques in Determining Bulk Properties of Tuffaceaous Rocks, SAND92-0119, Sandia National Laboratories, Albuquerque, NM.

Brechtel, C.E., M. Lin, E. Martin, and D. S. Kessel, 1995, Geotechnical Characterization of the North Ramp of the Exploratory studies, Facility, Yucca Mountain Site Characterization Project, SAND95-0488/2, Sandia National Laboratories, Albuquerque, NM.

Holcomb, D.J. and M. J. McNamee, 1984, Displacement Gage for the Rock Mechanics Laboratory, SAND84-0651, Sandia National Laboratories, Albuquerque, NM.

International Society for Rock Mechanics, 1981, Suggested Methods for Determining the Strength of Rock Materials in Triaxial Compression, In: *Rock Characterization Testing & Monitoring - ISRM Suggested Methods*, E.T. Brown (ed.), Pergamon Press, New York, 123-127.

Martin, R.J., III, R.H. Price, P.J. Boyd, and R.W. Haupt, 1992, Anisotrophy of the Topopah Spring Member Tuff, SAND91-0894, Sandia National Laboratories, Albuquerque, NM.

Martin, R.J., R.H. Price, P. J. Boyd, and J.S. Noel, 1994, Bulk and Mechanical Properties of the Paintbrush Tuff Recovered from Borehole USW NRG-6: Data Report, SAND93-4020, Sandia National Laboratories, Albuquerque, NM.

Martin, R.J., R.H. Price, P.J. Boyd, and J.S. Noel, 1995, Bulk and Mechanical Properties of the Paintbrush Tuff Recovered from Borehole USW NRG-7/7a: Data Report, SAND94-1996, Sandia National Laboratories, Albuquerque, NM.

Ortiz, T.S., R. L. Williams, F. B. Nimick, B. C. Whittet, and D. L. South, 1985, A Three-Dimensional Model of Reference Thermal/Mechanical and Hydrological Stratigraphy at Yucca Mountain, Southern Nevada, SAND84-1076, Sandia National Laboratories, Albuquerque, NM.

Price, R.H., and S. J. Bauer, 1985, Analysis of the Elastic and Strength Properties of Yucca Mountain Tuff, Nevada, In: *Research and Engineering Application in Rock Masses, Proceedings of the 26th U. S. Symposium on Rock Mechanics*, Eileen Ashworth (ed.), A.A. Balkema, Boston, MA, Vol. 1, 89-96.

Price, R.H., R.J. Martin, and R.W. Haupt, 1994, The Effect of Frequency on Young's Modulus and Seismic Wave Attenuation, SAND92-0847, Sandia National Laboratories, Albuquerque, NM.

Scott, R.B., and J. Bonk, 1984, Preliminary Geologic Map of Yucca Mountain, Nye County, Nevada, with Geologic Sections, USGS-OFR-84-494, U. S. Geological Survey, Denver, CO.

APPENDIX I

Stress vs Axial Strain and Radial Strain vs Axial Strain Plots for Confined Compression Experiments

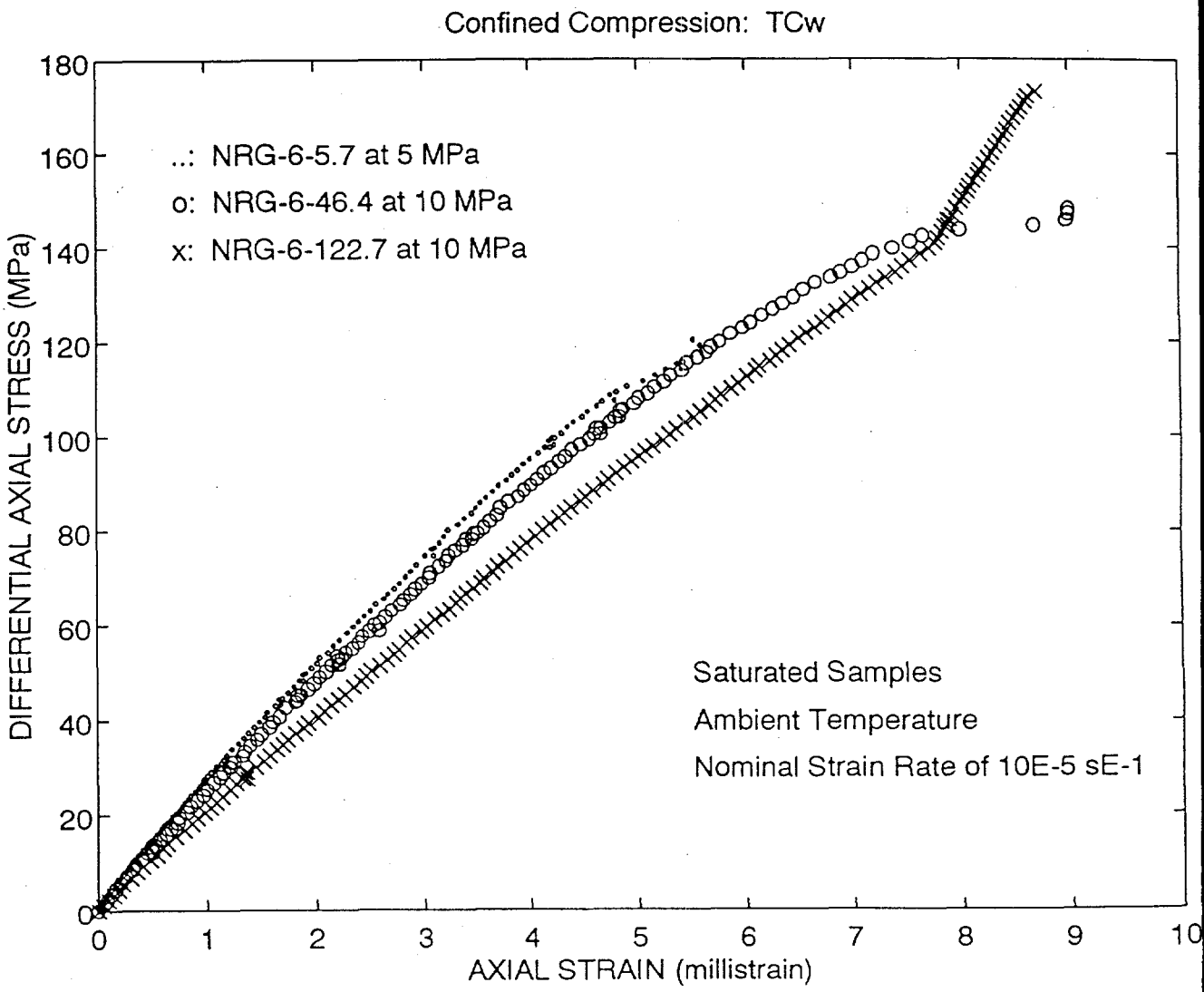

Figure A-I-1 Differential stress is plotted as a function of axial strain for tuff specimens tested in confined compression.

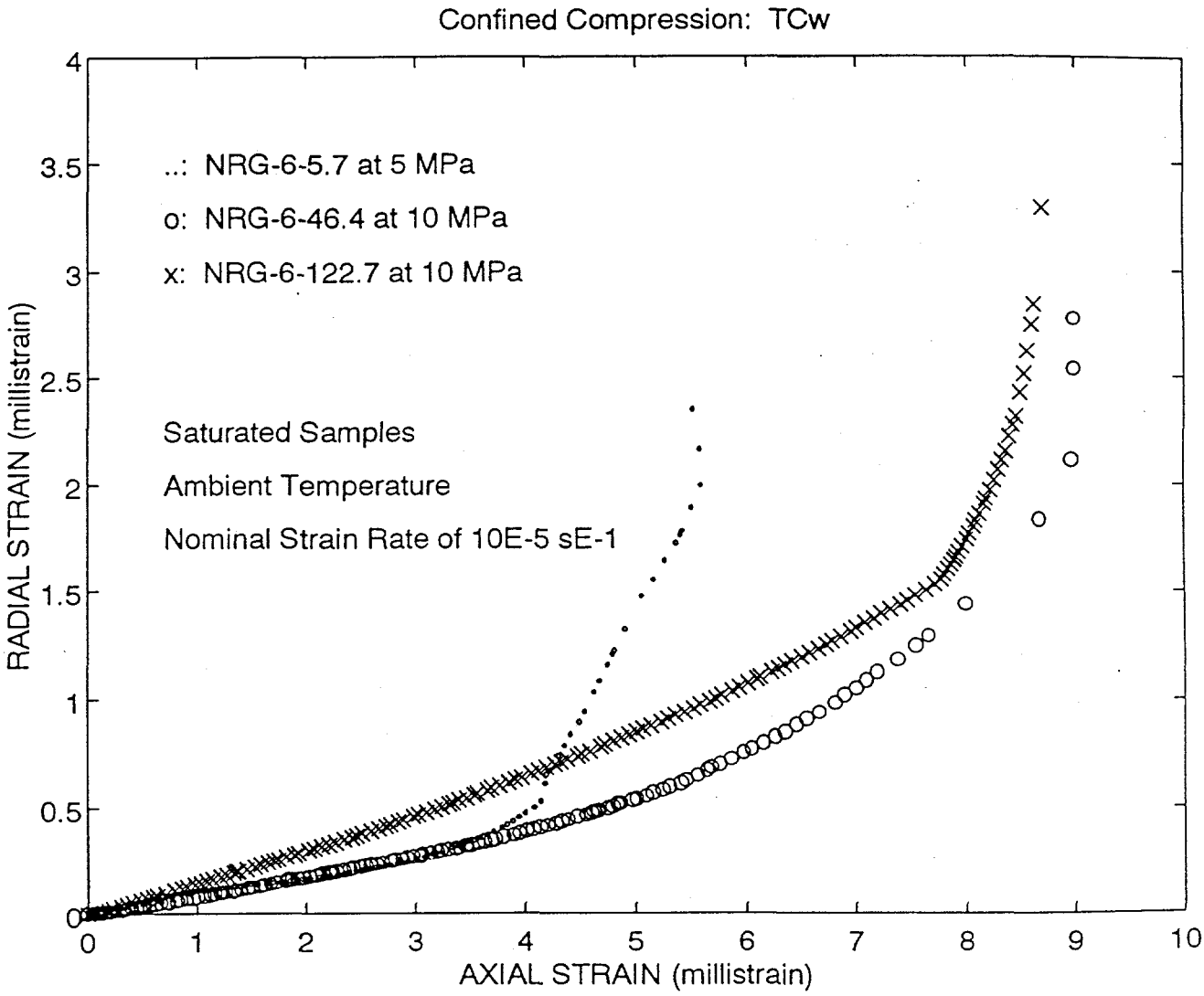

Figure A-I-2 Radial strain is plotted as a function of axial strain for tuff specimens tested in confined compression.

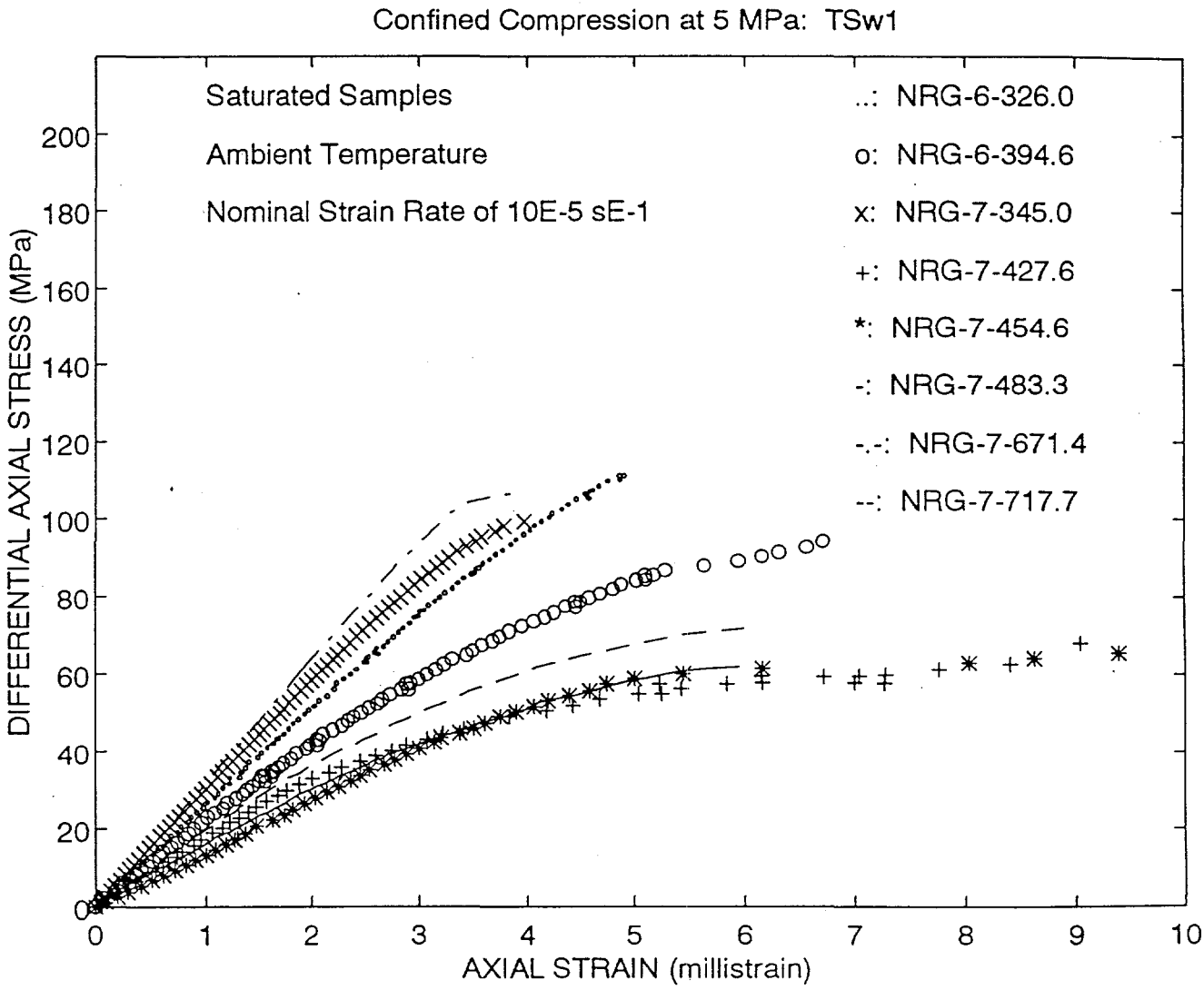

Figure A-I-3 Differential stress is plotted as a function of axial strain for tuff specimens tested in confined compression.

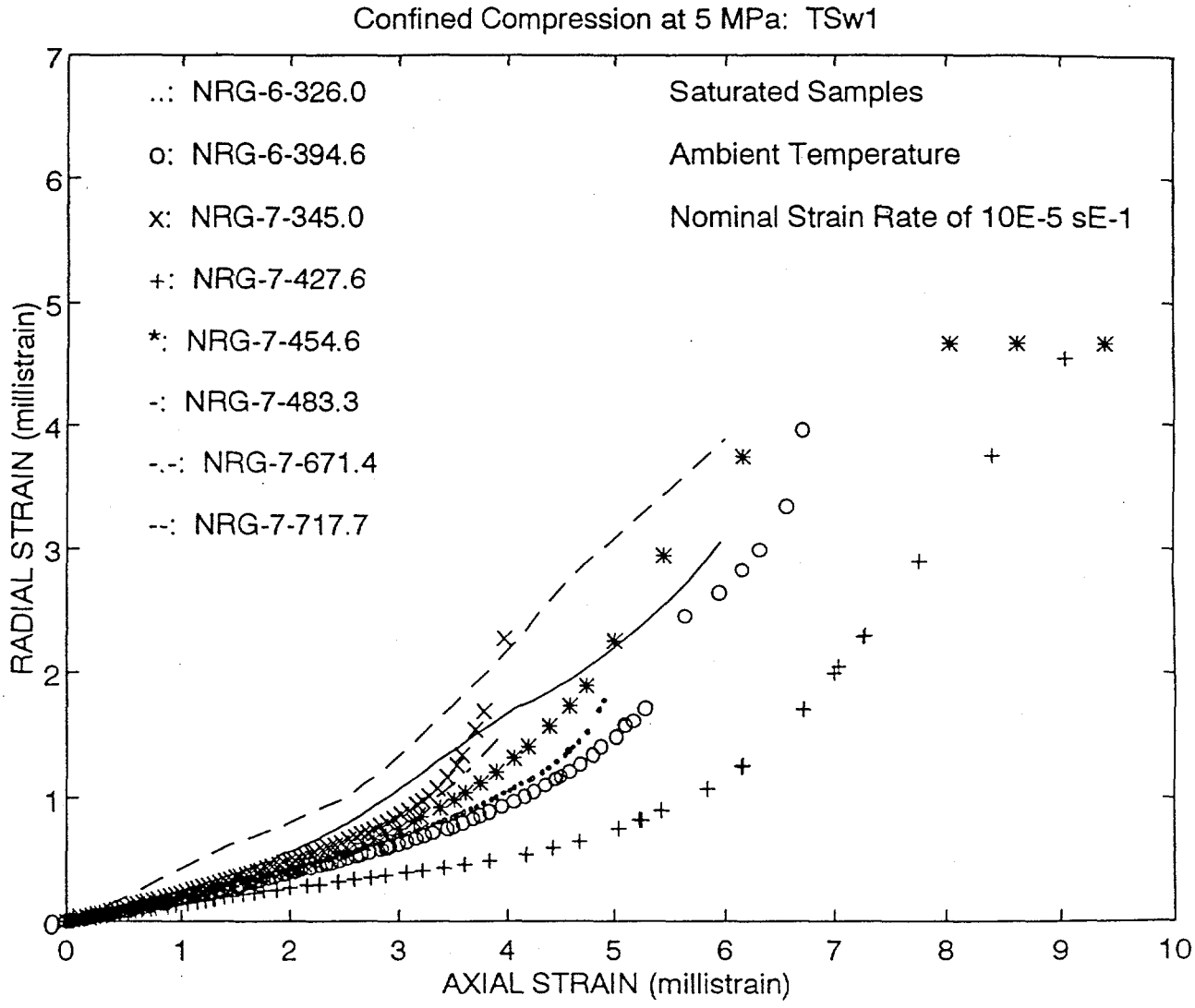

Figure A-I-4 Radial strain is plotted as a function of axial strain for tuff specimens tested in confined compression.

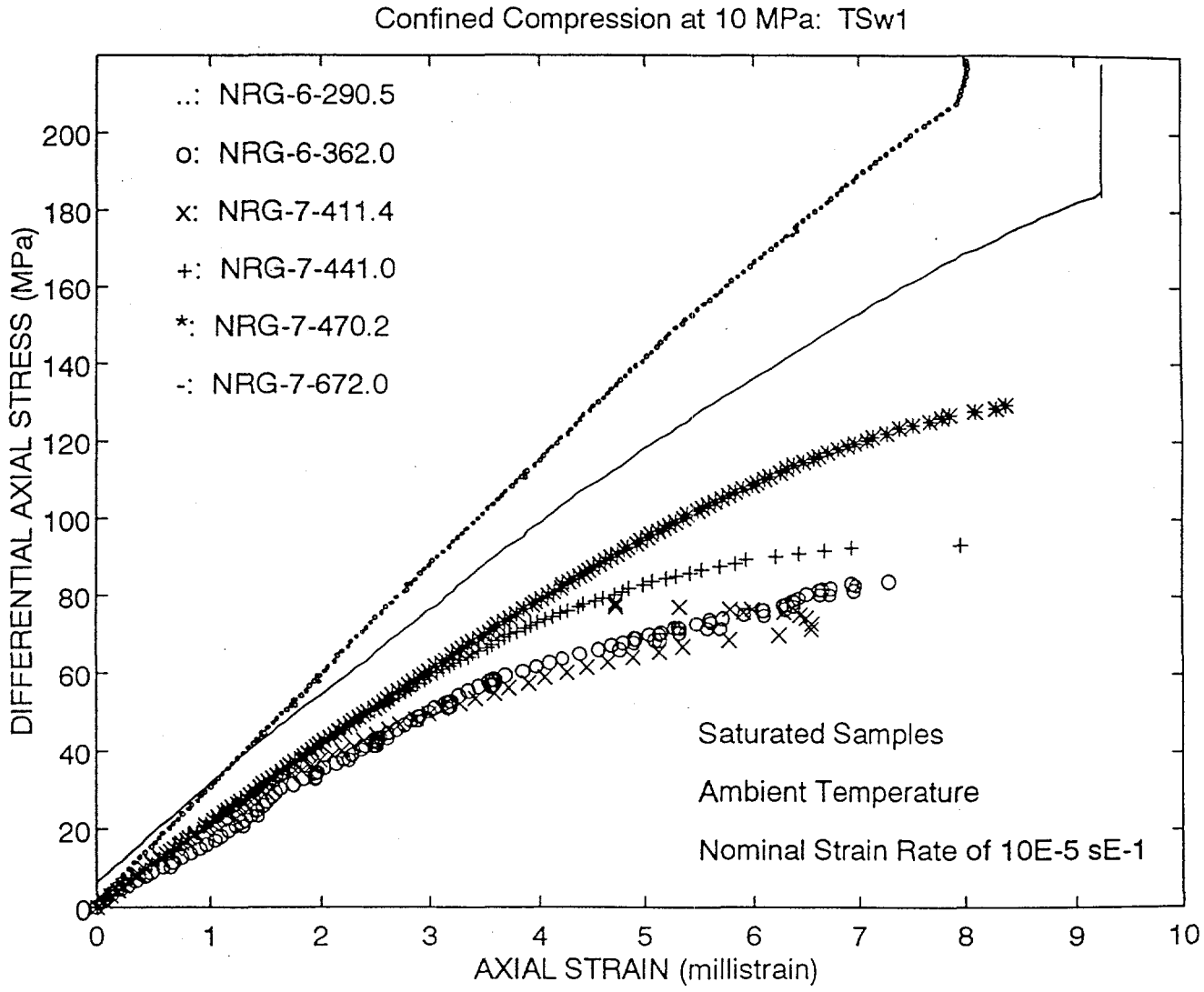

Figure A-I-5 Differential stress is plotted as a function of axial strain for tuff specimens tested in confined compression.

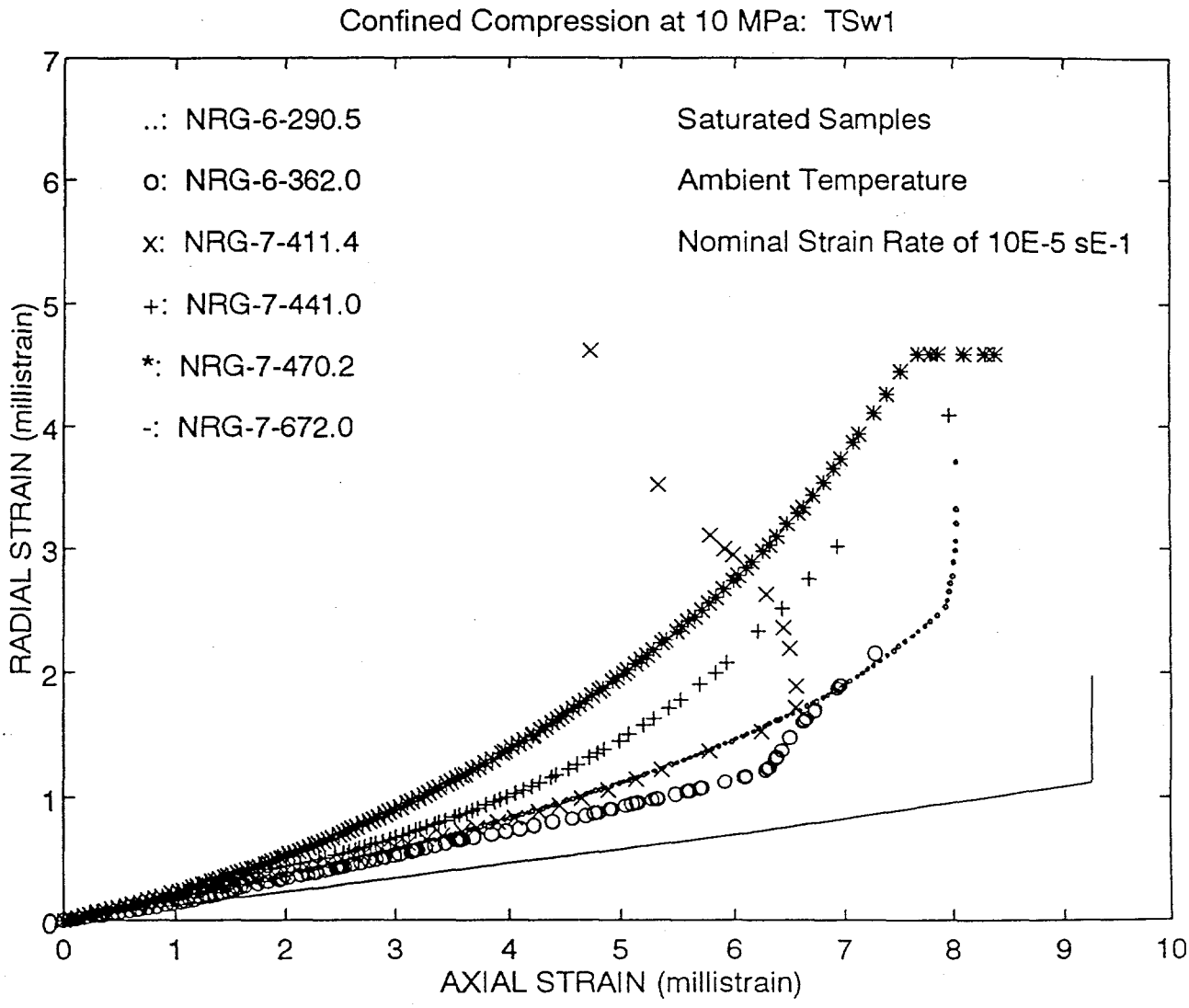

Figure A-I-6 Radial strain is plotted as a function of axial strain for tuff specimens tested in confined compression.

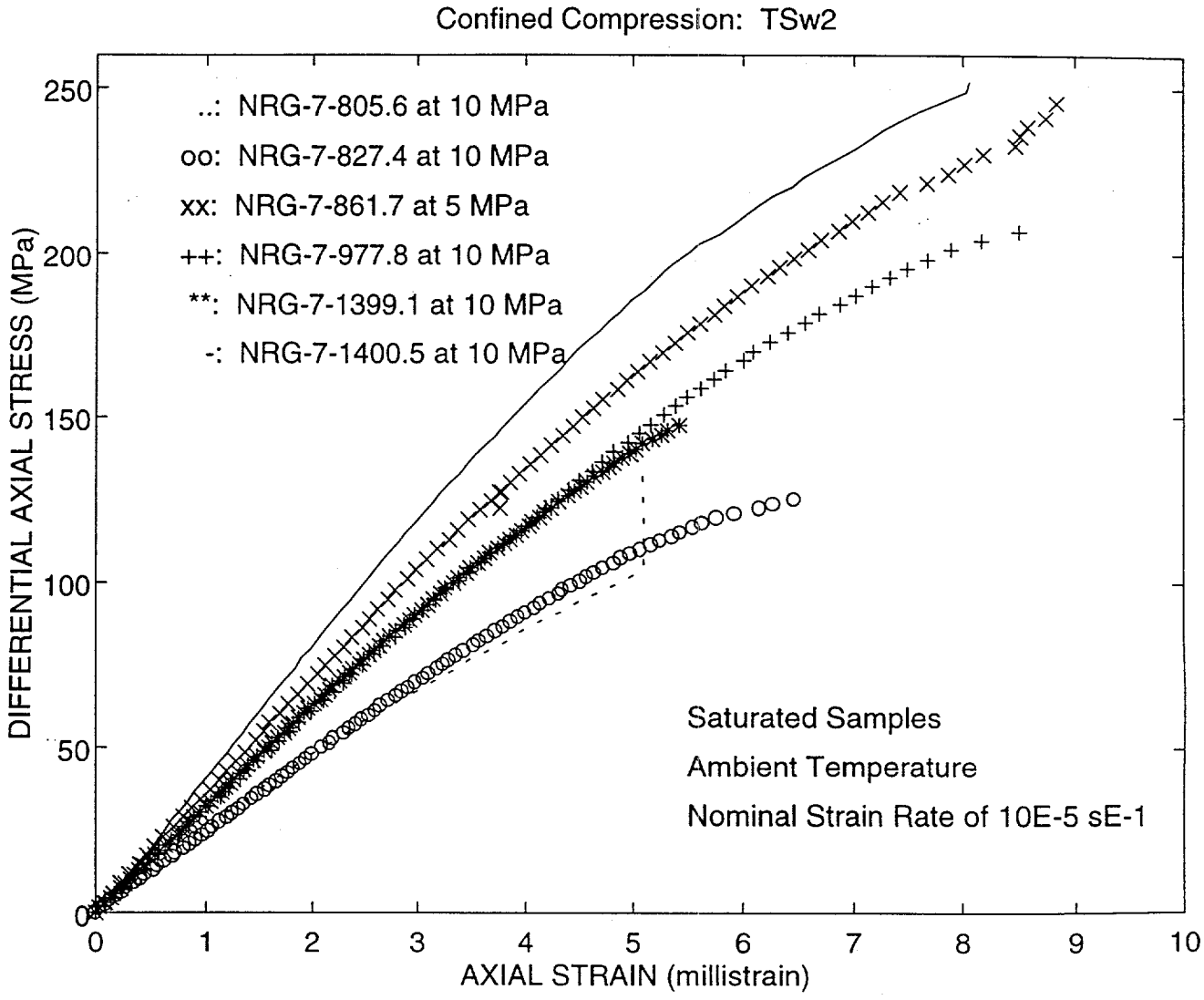

Figure A-I-7 Differential stress is plotted as a function of axial strain for tuff specimens tested in confined compression.

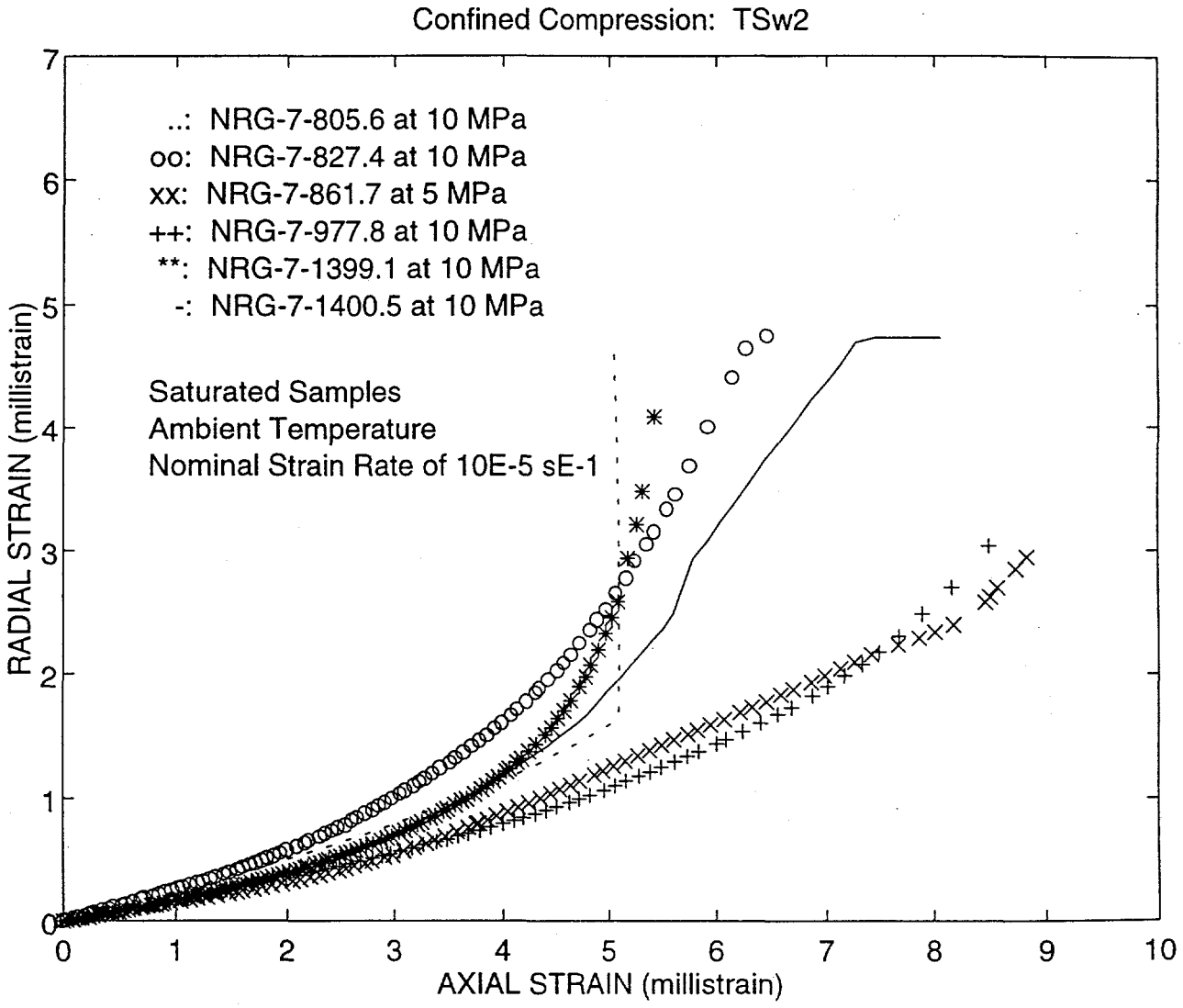

Figure A-I-8 Radial strain is plotted as a function of axial strain for tuff specimens tested in confined compression.

APPENDIX II

System Checks Using an Aluminum Standard Specimen

System Checks Using an Aluminum Standard Specimen

Unconfined compression experiments were performed on a specimen of 6061-T6511 aluminum. The specimen was monotonically loaded at a constant strain rate of 10^{-5} s^{-1} to 138 MPa, (i.e., approximately one-half of its yield stress). Young's modulus and Poisson's ratio were computed from the stress and strain data. The purpose of the system checks is to ensure that the entire system is performing correctly and that the reported data are accurate.

A system check involves performing the uniaxial compression experiment on aluminum and comparing the observed Young's modulus and Poisson's ratio with the standard values reported for the material. If the measured values deviate by more than ± 5 percent from the published reference values, corrective measures are taken and no further experiments are performed on tuff until the aluminum calibration experiment yields acceptable elastic constants.

Typical results from a calibration experiment are shown in Figure A-1. Axial stress and radial strain are plotted as a function of axial strain for an aluminum specimen with the same nominal dimensions as the tuff. These data were collected using the procedure specified for the unconfined compression experiments. The specimen is cyclically loaded to one-half its yield stress at a strain rate of 10^{-5} s^{-1}; Young's modulus and Poisson's ratio are computed from the data.

A summary of the system checks performed during the course of the study of the specimens from the USW NRG-6 and USW NRG-7/7A boreholes are presented in Table A-1. The results indicate that the system performed within the specified accuracy during the course of the study.

Compressional and shear wave velocities were measured on the aluminum standard specimen. These data were used to compute the dynamic Young's modulus and Poisson's ratio. These values are also shown in Table A-1. The fact that these values for both Young's modulus and Poisson's ratio are larger than those given in the literature, suggests that there are minor variations in the properties of aluminum supplied by the manufacturer. The elastic moduli for nonporous materials are frequently computed from the compressional and shear wave velocities. These dynamic values should be used in conjunction with the static measurements . In many cases, the manufacturer's data are obtained for tension experiments and empirically corrected for compression, which can also lead to a discrepancy.

Table A-II

USW NRG-6 and USW NRG-7/7A
System Checks
Aluminum Standard - 6061 T6511

Date	Young's Modulus GPa	Deviation %	Poisson's Ratio	Deviation %
29-Aug-94	71.95	3.2%	0.337	2.1%
14-Dec-94	67.88	-2.6%	0.320	-3.0%
16-Dec-95	66.81	-4.3%	0.321	-2.7%
8-Feb-95	68.7	-1.4%	0.333	0.9%
29-Jun-95	69.63	0.0%	0.33	0.0%
Reference	69.66		0.33	
Dynamic	71.02		0.34	

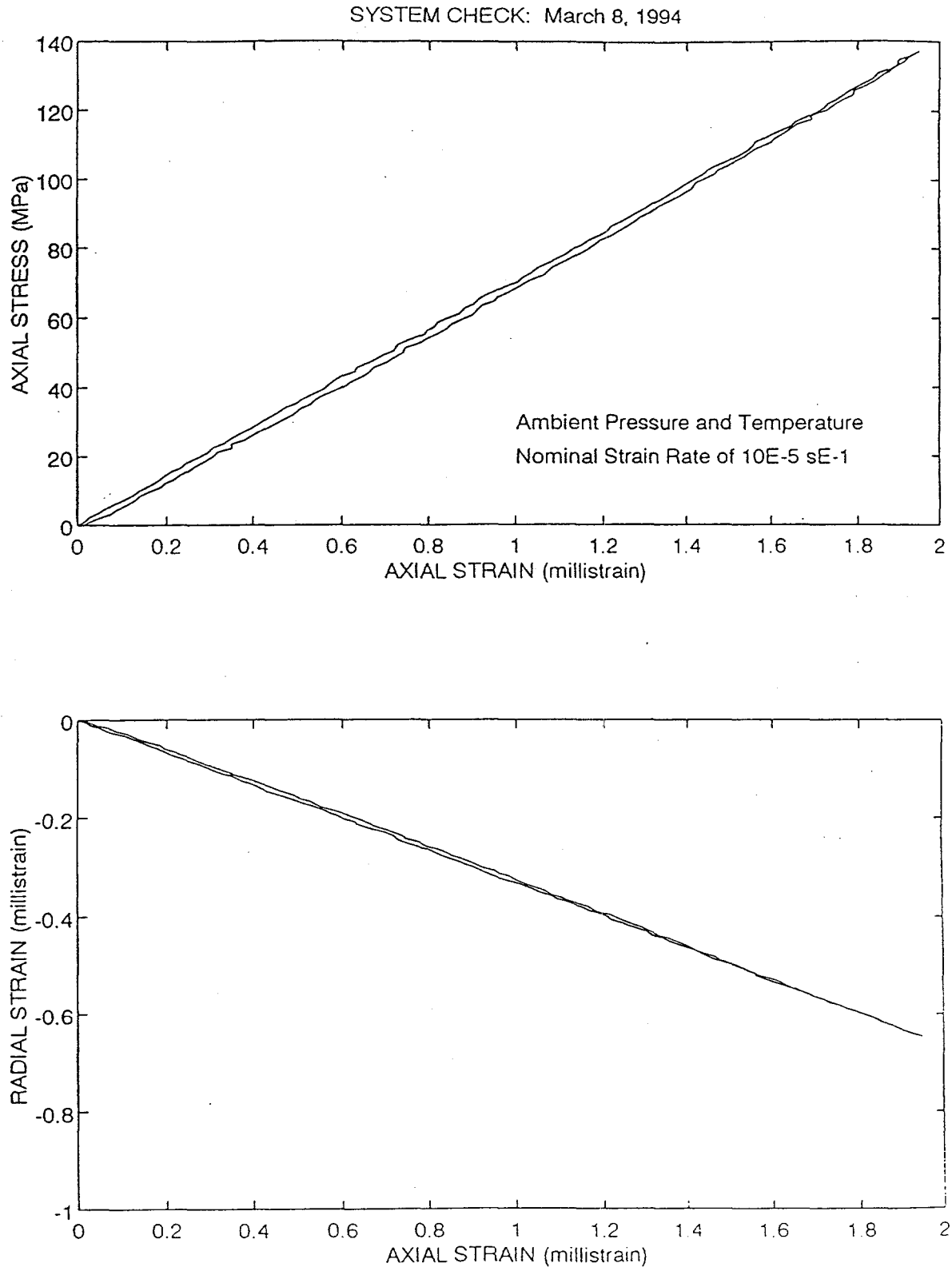

Figure A-II-1: Axial stress and radial strain are plotted as a function of axial strain for a specimen of 6061-T6511 aluminum cyclically loaded in unconfined compression.

APPENDIX III

Information from the Reference Information Base Used in this Report

This report contains no information from the Reference Information Base.

Candidate Information for the Reference Information Base

This report contains no information for the Reference Information Base.

Candidate Information for the Geographic Nodal Information Study and Evaluation System

This report contains candidate information for the Geographic Nodal Information Study and Evaluation System (GeNESIS) in Tables 1, 2, 3, 4, and 5. The data have been submitted to the SNL Participant Data Archive (PDA) and are indexed in the Automated Technical Data Tracking system (ATDT). The data packages have the following Data Tracking Numbers (DTN): SNL02030193001.021 and SNL02030193001.022.

YUCCA MOUNTAIN SITE CHARACTERIZATION PROJECT
SAND97-1887 - DISTRIBUTION LIST

1 D. A. Dreyfus (RW-1)
Director
OCRWM
US Department of Energy
1000 Independence Avenue SW
Washington, DC 20585

1 L. H. Barrett (RW-2)
Acting Deputy Director
OCRWM
US Department of Energy
1000 Independence Avenue SW
Washington, DC 20585

1 S. Rousso (RW-40)
Office of Storage and Transportation
OCRWM
US Department of Energy
1000 Independence Avenue SW
Washington, DC 20585

1 R. A. Milner (RW-30)
Office of Program Management
and Integration
OCRWM
US Department of Energy
1000 Independence Avenue SW
Washington, DC 20585

1 D. R. Elle, Director
Environmental Protection Division
DOE Nevada Field Office
US Department of Energy
P.O. Box 98518
Las Vegas, NV 89193-8518

1 T. Wood (RW-14)
Contract Management Division
OCRWM
US Department of Energy
1000 Independence Avenue SW
Washington, DC 20585

4 Victoria F. Reich, Librarian
Nuclear Waste Technical Review Board
1100 Wilson Blvd., Suite 910
Arlington, VA 22209

1 Wesley Barnes, Project Manager
Yucca Mountain Site Characterization
Office
US Department of Energy
P.O. Box 30307 MS 523
Las Vegas, NV 89036-0307

1 Director, Public Affairs Office
c/o Technical Information Resource Center
DOE Nevada Operations Office
US Department of Energy
P.O. Box 98518
Las Vegas, NV 89193-8518

8 Technical Information Officer
DOE Nevada Operations Office
US Department of Energy
P.O. Box 98518
Las Vegas, NV 89193-8518

1 J. R. Dyer, Deputy Project Manager
Yucca Mountain Site Characterization Office
US Department of Energy
P.O. Box 30307 MS 523
Las Vegas, NV 89036-0307

1 S. A. Orrell
Laboratory Lead for YMP
M&O/Sandia National Laboratories
1180 Town Center Dr.
Las Vegas, NV 89134

1 J. A. Canepa
Laboratory Lead for YMP
EES-13, Mail Stop J521
M&O/Los Alamos National Laboratory
P.O. Box 1663
Los Alamos, NM 87545

1 Repository Licensing & Quality
Assurance
Project Directorate
Division of Waste Management, MS T7J-9
US NRC
Washington, DC 20555

1 Senior Project Manager for Yucca
Mountain
Repository Project Branch
Division of Waste Management, MS T7J-9
US NRC
Washington, DC 20555

1 NRC Document Control Desk
Division of Waste Management, MS T7J-9
US NRC
Washington, DC 20555

1 Chad Glenn
NRC Site Representative
301 E Stewart Avenue, Room 203
Las Vegas, NV 89101

1 Center for Nuclear Waste
Regulatory Analyses
Southwest Research Institute
6220 Culebra Road
Drawer 28510
San Antonio, TX 78284

2 W. L. Clarke
Laboratory Lead for YMP
M&O/ Lawrence Livermore Nat'l Lab
P.O. Box 808 (L-51)
Livermore, CA 94550

1 Robert W. Craig
Technical Project Officer
US Geological Survey
1180 Town Center Dr.
Las Vegas, NV 89134

1 J. S. Stuckless,
Senior Science Advisor
MS 425
Yucca Mountain Project Branch
US Geological Survey
P.O. Box 25046
Denver, CO 80225

1 L. D. Foust, Asst. General Mgr.
Nevada Site
TRW Environmental Safety Systems
1180 Town Center Dr.
Las Vegas, NV 89134

1 A. L. Flint
U. S. Geological Survey
1180 Town Center Dr.
Las Vegas, NV 89134

1 Robert L. Strickler
Vice President & General Manager
TRW Environmental Safety Systems, Inc.
2650 Park Tower Dr.
Vienna, VA 22180

1 Jim Krulik, Technical Program Officer
US Bureau of Reclamation
Code D-8322
P.O. Box 25007
Denver, CO 80225-0007

1 B. T. Brady
Records Specialist
US Geological Survey
MS 421
P.O. Box 25046
Denver, CO 80225

1 M. D. Voegele
Deputy of Technical Operations
M&O/SAIC
1180 Town Center Dr.
Las Vegas, NV 89134

2 A. T. Tamura
Science and Technology Division
OSTI
US Department of Energy
P.O. Box 62
Oak Ridge, TN 37831

1 P. J. Weeden, Acting Director
Nuclear Radiation Assessment Div.
US EPA
Environmental Monitoring Sys. Lab
P.O. Box 93478
Las Vegas, NV 89193-3478

1 John Fordham, Deputy Director
Water Resources Center
Desert Research Institute
P.O. Box 60220
Reno, NV 89506

1 The Honorable Jim Regan
Chairman
Churchill County Board of
Commissioners
10 W. Williams Avenue
Fallon, NV 89406

1 R. R. Loux
Executive Director
Agency for Nuclear Projects
State of Nevada
Evergreen Center, Suite 252
1802 N. Carson Street
Carson City, NV 89710

1 Brad R. Mettam
Inyo County Yucca Mountain
Repository Assessment Office
P. O. Drawer L
Independence, CA 93526

1 Vernon E. Poe
Office of Nuclear Projects
Mineral County
P.O. Box 1600
Hawthorne, NV 89415

1 Les W. Bradshaw
Program Manager
Nye County Nuclear Waste Repository
Project Office
P.O. Box 1767
Tonopah, NV 89049

1 Florindo Mariani
White Pine County Coordinator
P. O. Box 135
Ely, NV 89301

1 Tammy Manzini
Lander County Yucca Mountain
Information Officer
P.O. Box 10
Austin, NV 89310

1 Jason Pitts
Lincoln County Nuclear Waste
Program Manager
P. O. Box 158
Pioche, NV 89043

1 Dennis Bechtel, Coordinator
Nuclear Waste Division
Clark County Dept. of Comprehensive
Planning
P.O. Box 55171
Las Vegas, NV 89155-1751

1 Juanita D. Hoffman
Nuclear Waste Repository
Oversight Program
Esmeralda County
P.O. Box 490
Goldfield, NV 89013

1 Sandy Green
Yucca Mountain Information Office
Eureka County
P.O. Box 714
Eureka, NV 89316

1 Economic Development Dept.
City of Las Vegas
400 E. Stewart Avenue
Las Vegas, NV 89101

1 Community Planning & Development
City of North Las Vegas
P.O. Box 4086
North Las Vegas, NV 89030

2 Librarian
YMP Research & Study Center
1180 Town Center Dr.
Las Vegas, NV 89134

1 Library Acquisitions
Argonne National Laboratory
Building 203, Room CE-111
9700 S. Cass Avenue
Argonne, IL 60439

1 Glenn Van Roekel
Manager, City of Caliente
P.O. Box 158
Caliente, NV 89008

1 G. S. Bodvarsson
Head, Nuclear Waste Department
Lawrence Berkeley National Laboratory
1 Cyclotron Road, MS 50E
Berkeley, CA 94720

1 Steve Hanauer (RW-2)
OCRWM
U. S. Department of Energy
1000 Independence Ave.
Washington, DC 20585

5 Randolph J. Martin III
New England Research
76 Olcott Drive
White River, VT 05001

1 Robert W. Clayton
M&O/WCFS
1180 Town Center Drive/MS423
Las Vegas. NV 89134

1 Richard C. Quitmeyer
M&O/WCFS
1180 Town Center Drive/MS423
Las Vegas, NV 89134

1 Mark C. Tynan
DOE/YMPSCO
1180 Town Center Drive/MS523/HL
Las Vegas, NV 89134

	MS	
15	1325	R. H. Price, 6811
5	0751	N. Brodsky, 6117
1	0751	L. S. Costin, 6117
5	1399	D. S. Kessel, 6850
2	1330	K. Hart, 6811 100/1232713/SAND95-1887QA
20	1330	WMT Library, 6752
1	9018	Central Technical Files, 8940-2
5	0899	Technical Library, 4414
2	0619	Review and Approval Desk, 12690, For DOE/OSTI